

See discussions, stats, and author profiles for this publication at: <https://www.researchgate.net/publication/221745685>

Conformational Dynamics of Abasic DNA upon Interactions with AP Endonuclease 1 Revealed by Stopped-Flow Fluorescence Analysis

ARTICLE in BIOCHEMISTRY · FEBRUARY 2012

Impact Factor: 3.02 · DOI: 10.1021/bi201444m · Source: PubMed

CITATIONS

10

READS

33

4 AUTHORS, INCLUDING:



Vladimir V Koval

Institute of Chemical Biology and Fundament...

51 PUBLICATIONS 504 CITATIONS

SEE PROFILE



Yu. N. Vorob'ev

Russian Academy of Sciences

32 PUBLICATIONS 802 CITATIONS

SEE PROFILE



Olga S Fedorova

Institute of Chemical Biology and Fundament...

125 PUBLICATIONS 1,078 CITATIONS

SEE PROFILE

Conformational Dynamics of Abasic DNA upon Interactions with AP Endonuclease 1 Revealed by Stopped-Flow Fluorescence Analysis

Lyubov Yu. Kanazhevskaya,[†] Vladimir V. Koval,^{†,‡} Yury N. Vorobjev,^{†,‡} and Olga S. Fedorova^{*,†,‡}

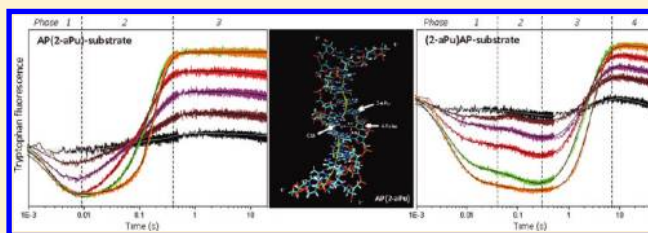
[†]Institute of Chemical Biology and Fundamental Medicine, Siberian Branch of the Russian Academy of Sciences, Novosibirsk 630090, Russia

[‡]Novosibirsk State University, Novosibirsk 630090, Russia

Supporting Information

ABSTRACT: Apurinic/aprimidinic (AP) sites are abundant DNA lesions arising from exposure to UV light, ionizing radiation, alkylating agents, and oxygen radicals. In human cells, AP endonuclease 1 (APE1) recognizes this mutagenic lesion and initiates its repair via a specific incision of the phosphodiester backbone 5' to the AP site. We have investigated a detailed mechanism of APE1 functioning using fluorescently labeled DNA substrates. A fluorescent adenine analogue, 2-aminopurine, was introduced into DNA substrates

adjacent to the abasic site to serve as an on-site reporter of conformational transitions in DNA during the catalytic cycle. Application of a pre-steady-state stopped-flow technique allows us to observe changes in the fluorescence intensity corresponding to different stages of the process in real time. We also detected an intrinsic Trp fluorescence of the enzyme during interactions with 2-aPu-containing substrates. Our data have revealed a conformational flexibility of the abasic DNA being processed by APE1. Quantitative analysis of fluorescent traces has yielded a minimal kinetic scheme and appropriate rate constants consisting of four steps. The results obtained from stopped-flow data have shown a substantial influence of the 2-aPu base location on completion of certain reaction steps. Using detailed molecular dynamics simulations of the DNA substrates, we have attributed structural distortions of AP-DNA to realization of specific binding, effective locking, and incision of the damaged DNA. The findings allowed us to accurately discern the step that corresponds to insertion of specific APE1 amino acid residues into the abasic DNA void in the course of stabilization of the precatalytic complex.



AP endonuclease 1 (APE1, HAP1, APEX, ref-1) is a key enzyme of the base excision repair (BER) pathway in human cells, which recognizes apurinic/aprimidinic (AP) sites in double-stranded DNA and makes a single nick in the phosphodiester backbone 5' to the AP site.^{1,2} APE1 operates at the second step of the BER pathway after the removal of the damaged base by specific DNA glycosylases.³ The resulting 3'-OH moiety is recognized and processed by DNA polymerase β .⁴ Because AP sites that arise through hydrolysis of N-glycosidic bonds of abnormal bases are highly mutagenic and cytotoxic for living cells, the correct functioning of APE1 during the repair process is extremely important.⁵ APE1 was also shown to cleave DNA near some base-containing damaged deoxynucleotides in a nucleotide incision repair (NIR) process.⁶ Besides DNA repair, APE1 participates in the regulation of transcription factors such as p53, HIF-1 α , and AP-1 (Fos/Jun) involved in cancer promotion and progression through reduction-oxidation signaling.^{7–11} The redox activity of APE1 is mediated by Cys⁶⁵, Cys⁹³, and Cys³¹⁰ and is important for sensitizing cancer cells to chemotherapeutic agents.^{12,13}

The endonuclease activity of APE1 in the BER process has been investigated over the past 15 years. Several hypotheses explaining how DNA recognition, binding, and incision steps

are conducted by this enzyme exist. As a member of the ExoIII family, this enzyme incises the phosphodiester backbone by a Mg²⁺-dependent acid-base S_N2 hydrolysis. A recently published study suggests that APE1 acts by means of a one-step associative mechanism in which an activated water molecule serves as an attacking nucleophile, resulting in the formation of an unstable pentacoordinate transition state.¹⁴ This stage is immediately followed by expulsion of the 5' leaving group and cleavage of the phosphodiester bond. High-resolution crystal structures and footprinting studies of APE1 in a complex with abasic or incised DNA or without DNA have provided important insights into the active site pocket structure and amino acid residues participating in cleavage of the target bond.^{15–18} However, crystallographic data cannot reveal probable transient states of the enzyme and DNA that arise during the conversion of the APE1–DNA recognition complex into the complex with products. Although many biochemical and site-directed mutagenesis studies have defined general properties of the APE1 catalytic reaction, consensus has not yet been reached. In particular, several hypotheses of the abasic site

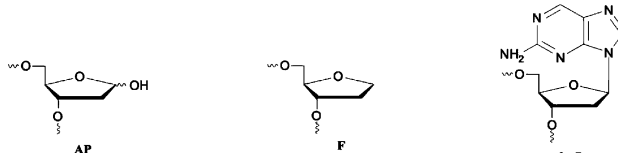
Received: September 16, 2011

Revised: January 12, 2012

Published: January 13, 2012



Table 1. Sequences of Oligonucleotides Used in This Study

Name	Substrate sequence
AP (or F)	5'-d(C ₁ T ₂ C ₃ T ₄ C ₅ AP ₆ C ₇ C ₈ T ₉ T ₁₀ C ₁₁ C ₁₂) 3' / 5'-d(G ₁₃ G ₁₄ A ₁₅ A ₁₆ G ₁₇ G ₁₈ C ₁₉ G ₂₀ A ₂₁ G ₂₂ A ₂₃ G ₂₄) 3'
AP(2-aPu)	5'-d(C ₁ T ₂ C ₃ T ₄ C ₅ AP ₆ (2-aPu) ₇ C ₈ T ₉ T ₁₀ C ₁₁ C ₁₂) 3' / 5'-d(G ₁₃ G ₁₄ A ₁₅ A ₁₆ G ₁₇ C ₁₈ C ₁₉ G ₂₀ A ₂₁ G ₂₂ A ₂₃ G ₂₄) 3'
(2-aPu)AP	5'-d(C ₁ T ₂ C ₃ T ₄ (2-aPu) ₅ AP ₆ C ₇ C ₈ T ₉ T ₁₀ C ₁₁ C ₁₂) 3' / 5'-d(G ₁₃ G ₁₄ A ₁₅ A ₁₆ G ₁₇ G ₁₈ C ₁₉ C ₂₀ A ₂₁ G ₂₂ A ₂₃ G ₂₄) 3'
F(2-aPu)	5'-d(C ₁ T ₂ C ₃ T ₄ C ₅ F ₆ (2-aPu) ₇ C ₈ T ₉ T ₁₀ C ₁₁ C ₁₂) 3' / 5'-d(G ₁₃ G ₁₄ A ₁₅ A ₁₆ G ₁₇ C ₁₈ C ₁₉ G ₂₀ A ₂₁ G ₂₂ A ₂₃ G ₂₄) 3'
(2-aPu)F	5'-d(C ₁ T ₂ C ₃ T ₄ (2-aPu) ₅ F ₆ C ₇ C ₈ T ₉ T ₁₀ C ₁₁ C ₁₂) 3' / 5'-d(G ₁₃ G ₁₄ A ₁₅ A ₁₆ G ₁₇ G ₁₈ C ₁₉ C ₂₀ A ₂₁ G ₂₂ A ₂₃ G ₂₄) 3'
Chemical nature of atypical nucleosides	
	

specific recognition are discussed. Some of them are based on identification of an extrahelical DNA moiety such as abasic deoxyribose sugar or an “orphan” base opposite the AP site.^{16,19} Other authors suggest a local DNA distortion produced by the AP site or a DNA conformational change upon protein binding as unique signals for the APE1 enzyme.^{20,21} Recently, a Trp²⁸⁰ side chain of the protein was reported to intercalate into the lesion pocket during specific recognition of the damage.²²

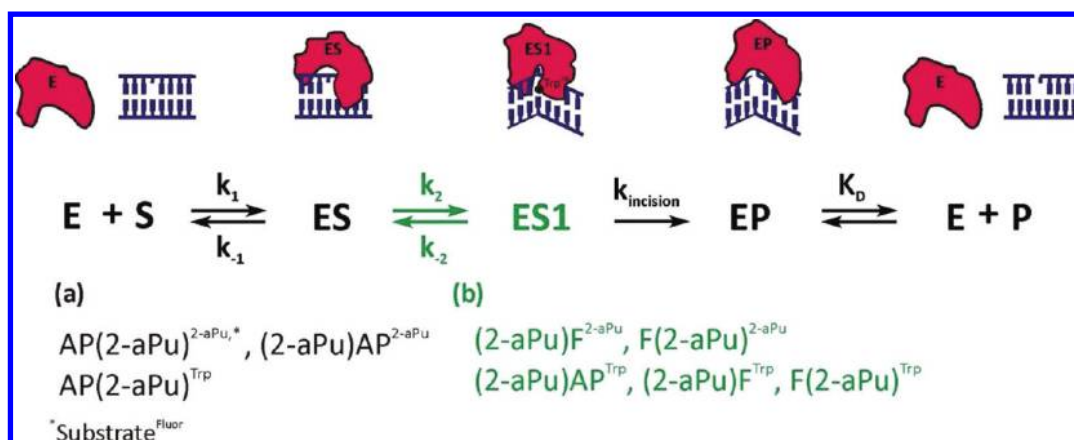
Understanding the reaction mechanism along with transient states and conformational dynamics of APE1 is important for the design of inhibitors, which have been shown to increase the efficacy of cancer chemotherapeutics.^{23–25} The experiments performed under steady-state multiple-turnover conditions have determined Michaelis–Menten parameters for DNA substrates of different lengths and specificities.^{26–29} Studies of APE1 in a complex with intact or incised AP-DNA suggests that the product DNA forms a stable complex with the enzyme and even serves as a competitive inhibitor for APE1.³⁰ The results demonstrated that phosphodiester backbone cleavage catalyzed by APE1 cannot be described by a simple first-order reaction scheme,^{16,27} and thus, clarification of the mechanism and the enzyme transient states required transient kinetic approaches. Recently, the first pre-steady-state analysis of APE1 has been published.³¹ Using a quench-flow technique, the authors reported the existence of a slow step that occurred after chemistry, but before dissociation of the product, which limited the steady-state incision rate of an extremely fast APE1 reaction (at least 850 s^{−1}) to 2–10 s^{−1}. The approach applied has provided significant, new insights into the APE1 kinetic mechanism. However, monitoring the reaction proceeding by accumulated products precludes registration of important events taking place within the active site before the product is formed. An alternative pre-steady-state kinetic approach is a stopped-flow assay combined with the fluorescence measurements. Stopped-flow studies have been widely reported in the literature as a powerful approach to defining elementary steps of enzymatic reaction pathways.^{32–36}

In our previous work, we applied the stopped-flow method to detect conformational transitions and transient states of the APE1 molecule corresponding to particular steps of the catalytic cycle, under single-turnover conditions.³⁷ Conformational dynamics within the enzyme active site was monitored in real time using changes in Trp fluorescence intensity. Our data have revealed a high level of flexibility of the APE1 molecule and complexity of the catalytic process. As a result, we proposed a four-step kinetic mechanism of abasic DNA

cleavage, including nonspecific encounter complex formation, mutual adjustment of the enzyme and DNA structures for catalysis, catalytic incision of the substrate, and release of APE1 from its complex with products. Using different types of DNA substrates, containing a natural AP site or tetrahydrofuran (F), we discovered that a C1'-hydroxyl moiety of the abasic sugar plays an important role in AP-DNA coordination for effective catalysis.

Herein, we report a consistent extension of the APE1 investigation directed at registration of the DNA conformational dynamics. The main idea was that the abasic DNA helix may undergo conformational changes similar to those of the protein molecule that would provide more precise information about the nature of individual steps of the reported mechanism. To probe the conformational dynamics of damaged DNA, a 2-aminopurine (2-aPu) fluorescent nucleoside was introduced into 12-mer DNA duplexes so that it flanked the natural abasic site or its synthetic analogue, F. After APE1 had been rapidly mixed with DNA substrates, significant changes in the 2-aPu fluorescence intensity were observed, corresponding to the binding and incision steps of the mechanism. Then, a conformational dynamics of the enzyme was traced during the processing the 2-aPu-containing substrates, and the Trp fluorescent signal was excited and monitored separately from 2-aPu. Our data indicate that DNA cleavage catalyzed by APE1 is accompanied by coordinated structural rearrangements within the enzyme and DNA molecules. Comparison of 2-aPu and Trp fluorescence dynamics permits us to attribute more precisely conformational transitions within the enzyme–substrate complex to particular steps of the kinetic mechanism. On the basis of the findings, we propose the second step of the mechanism represents the process of abasic void filling by specific residues of APE1, including Trp²⁸⁰. The pre-steady-state kinetic results show a significant difference in the processing rate depending on the location of the 2-aPu probe. To associate the observed effect of DNA sequence context on APE1 reaction rate with the structural diversity of the substrates, we applied detailed molecular dynamic modeling. As a result, we have found that “better” DNA substrates show an increased level of motion of the helix bases and backbone. On the other hand, using the “slower” substrates with reduced levels of specific binding and catalysis rates allows us to discover new transient states of the APE1–DNA complex occurring before the incision step.

Scheme 1. Kinetic Mechanism for Abasic DNA Cleavage by the APE1 Protein Derived from the Stopped-Flow Fluorescence Data^a



^aThe substrates, for which the step of ES1 transient complex formation is not observed, are listed under (a). The substrates displaying three individual transient states of APE1 or DNA on the fluorescence curves are colored green and listed under (b). Abbreviations: E, APE1; S, free DNA substrate; ES, bimolecular encounter complex; ES1, subsequent state of the APE1–DNA complex; EP, complex of APE1 with the DNA product; P, product of substrate incision. Rate constants k_1 and k_2 characterize the forward reactions, whereas k_{-1} and k_{-2} are the rate constants for reverse reactions; $k_{incision}$ corresponds to the irreversible chemical step. K_D is an equilibrium dissociation constant for decay of the EP complex.

EXPERIMENTAL PROCEDURES

Oligonucleotide Synthesis and Purification. Oligodeoxyribonucleotides [ODNs (Table 1)] containing normal DNA bases, deoxyuridine, tetrahydrofuran, and 2-aminopurine, were synthesized on an ASM-700 synthesizer (BIOSSET Ltd., Novosibirsk, Russia) using phosphoramidites purchased from Glen Research (Sterling, VA) and purified by anion exchange high-performance liquid chromatography (HPLC) on a Nucleosil 100-10 N(CH₃)₂ column followed by reverse-phase HPLC on a Nucleosil 100-10 C₁₈ column (both columns from Macherey-Nagel, Düren, Germany). The concentrations of the ODNs were determined from their absorbance at 260 nm. The AP-containing ODN was prepared by incubation of the deoxyuridine-containing ODN (0.1 mmol) for 14 h at 37 °C with 15 units of uracil-DNA glycosylase in 150 μ L of 20 mM Tris-HCl (pH 8.0), 1 mM EDTA, 1 mM dithiothreitol (DTT), and 0.1 mg/mL bovine serum albumin as previously described.³⁸ A reverse-phase HPLC system on a Nucleosil 100-5 C₁₈ column was used to purify the reaction product, which had a retention time shorter than that of the starting oligonucleotide, using a linear gradient from 0 to 20% acetonitrile in 0.1 M triethylammonium acetate (pH 7.0). The pooled fractions were concentrated and then converted to the lithium salt form using a Sep-Pak Plus C₁₈ cartridge (Waters, Milford, MA). To confirm the presence of the AP site in the ODN after the treatment with uracil-DNA glycosylase, samples were treated with 10% aqueous piperidine at 95 °C or annealed to the complementary oligonucleotide and treated with APE1 under the conditions described below. A PAGE analysis indicated that in both cases the material was cleaved to two shorter oligonucleotides. The purity, homogeneity, and integrity of each ODN were proved by matrix-assisted laser desorption ionization time-of-flight mass spectroscopy and assessed by 20% PAGE after staining with Stains-All (Sigma-Aldrich, St. Louis, MO). When necessary, the modified strands were labeled with ³²P using [γ -³²P]ATP and bacteriophage T4 polynucleotide kinase (SibEnzyme) according to the manufacturer's protocol and purified by 20% denaturing PAGE. ODN duplexes were prepared by annealing the modified and

complementary strands in a molar ratio of 1:1. Under the conditions used for the stopped-flow experiments with a high Mg²⁺ concentration (see below), the predicted equilibrium constant of the duplex formation is $\sim 1 \times 10^9$ M⁻¹, suggesting that nearly 100% of the oligonucleotides are in the double-helix form.^{39–41}

APE1 Expression and Purification. The recombinant human APE1 was expressed in BL21(DE3) pLysS *Escherichia coli* cells from a pET11a plasmid carrying a wild-type *ape1* gene. The protein was purified using the previously described protocol.³⁷ The purity of APE1 was nearly 95% as judged from SDS–PAGE with Coomassie Blue staining.

Stopped-Flow Fluorescence Experiments. Stopped-flow fluorescence measurements were taken using a model SX.18MV stopped-flow spectrometer (Applied Photophysics, Leatherhead, U.K.) fitted with a 150 W Xe arc lamp. The excitation wavelengths (λ_{ex}) were 280 and 310 nm for tryptophan and 2-aminopurine, respectively. The emission of Trp fluorescence was followed at λ_{em} values of >320 nm using long-pass filter WG 320 (Schott, Mainz, Germany). The fluorescence of 2-aPu was followed at λ_{em} values of >370 nm (Corion filter LG-370). When 2-aPu was presented in ODNs, the fluorescence of the enzyme was monitored using Corion filter P10-340, which transmits a 10 nm wide band at ~ 340 nm.⁴² The P10-340 filter is effective for enriching the Trp fluorescence on a background of total fluorescence. According to our rough estimate, the contribution of 2-aminopurine to the total fluorescence when measured using this filter does not exceed 20% and cannot significantly distort the general pattern of the fluorescence curves. Typically, each trace shown is the average of at least five independent trials. All experiments were conducted at 25 °C in a reaction buffer containing 50 mM HEPES-KOH (pH 7.5), 20 mM KCl, 10 mM MgCl₂, and 2 mM DTT. The Trp fluorescence changes were observed with a constant enzyme concentration (1.5 μ M) and ODN concentrations that varied from 0.5 to 4 μ M. During the registration of 2-aPu fluorescence, the APE1 concentration was varied in range of 0.3–3.0 μ M, and the ODN's concentration was 1 μ M.

Bleaching of Enzyme Fluorescence. To correct the measured data for bleaching, the fluorescence intensities were recalculated using eq 1:

$$F = (F_{\text{obs}} - F_b) \times \exp(k_b t) + F_b \quad (1)$$

where F is the corrected fluorescence intensity, F_{obs} is the observed fluorescence intensity, F_b is the background fluorescence, and k_b is the coefficient determined for each substrate concentration in experiments with the noncleavable DNA duplex containing a G residue instead of AP or F.

Analysis of Pre-Steady-State Kinetic Data. A global nonlinear least-squares fitting was performed using DynaFit (BioKin, Pullman, WA).⁴³ Differential equations were written for each species in the mechanism described by Scheme 1 (see Results). The stopped-flow Trp fluorescence traces were directly fit by expressing the corrected fluorescence intensity (F_c) at any reaction time t as the sum of the background fluorescence (F_b) and the fluorescence intensities of each protein species:

$$F_c = F_b + \sum_{i=0}^n F_i(t) \quad (2)$$

where $F_i(t) = f_i[E_i(t)]$, f_i is the coefficient of specific fluorescence for each discernible APE1 conformer, and $E_i(t)$ is the concentration of the conformer at any given time t ($i = 0$ relates to the free protein and $i > 0$ to the protein–DNA complexes). These specific fluorescence coefficients describe only the part of fluorescence that changes as a result of DNA binding. Similar fitting procedures were used for 2-aPu fluorescence traces with the difference being that fluorescently discernible transient states corresponded to DNA species. The minimal nature of the reaction schemes was confirmed using a “scree test”.⁴⁴ Errors in all rate constant values measured by the stopped-flow assay did not exceed 30%.

Fluorescence Equilibrium Titration of APE1. To determine the dissociation constant K_D^{titr} of the complex of APE1 with the product of AP site incision, we titrated the enzyme with a mixture of the appropriate ODNs listed in Table 3. Each point on the fluorescence titration curve was obtained via measurement of the Trp fluorescence intensity of separate solutions (80 μL) containing APE1 (1.5×10^{-6} M) and the ODNs at the required concentration in the reaction buffer described above. The mixtures were incubated at 25 °C for 1 min, and the fluorescence spectra were recorded ($\lambda_{\text{ex}} = 280$ nm, and $\lambda_{\text{em}} = 330$ nm) using a Cary Eclipse fluorescence spectrophotometer (Varian). Three independent titrations were averaged, and the data were fit as described in ref 37. Data analysis was performed using Origin (Originlab Corp.). The value of the K_D^{titr} constant was determined from eq 3:

$$F = f_0 + f_2 e_0 + \frac{f_1 - f_2}{2} \left[\sqrt{(K_D^{\text{titr}} + p_0 - e_0)^2 + 4K_D^{\text{titr}} e_0} - K_D^{\text{titr}} - p_0 + e_0 \right] \quad (3)$$

where F is the Trp fluorescence intensity measured for each ODN concentration; f_0 , f_1 , and f_2 are fluorescence intensities of APE1 with no ODNs added, at any given ODN concentration, and at the saturating ODN concentration, respectively; e_0 and p_0 are the total concentrations of APE1 and the ODNs,

respectively; and K_D^{titr} is an equilibrium dissociation constant of decay of the enzyme–product complex.

Cleavage Time Course Experiments. The damaged DNA strands were 5'-labeled with ^{32}P and annealed to the complementary strand; 1.5 μM substrates were mixed with 1.5 μM enzyme in the reaction buffer containing 50 mM HEPES-KOH (pH 7.5), 20 mM KCl, 10 mM MgCl_2 , and 2 mM DTT. The reaction that was conducted at 25 °C was terminated at required time points by the addition of a loading dye solution containing 7 M urea. Aliquots were then analyzed by 20% denaturing PAGE, and the gels were imaged by autoradiography and quantified by scanning densitometry using Gel-Pro Analyzer version 4.0 (Media Cybernetics, Silver Spring, MD).

Molecular Dynamics Modeling. As a complement to stopped-flow studies, we performed six independent molecular dynamics (MD) simulations using BIOPASED.⁴⁵ Four MD simulations used 2-aPu-containing abasic DNA duplexes (see Table 1), and two of them used the same duplexes without 2-aPu, where the abasic site was flanked by cytosines (AP-substrate or F-substrate). The initial structure of each DNA dodecamer was built in a canonical B-form by HyperChem. To build the damaged AP- or F-containing DNA, a guanosine base was removed from the sixth position of the duplex. The initial structure of 2-aPu-containing DNA duplexes was built by replacing the guanosine residue with the 2-aPu base at the appropriate position. BIOPASED uses an AMBER99 all-atom force field⁴⁶ and implicit Gaussian shell (GS) solvation model.⁴⁷ The original GS model was extended to describe the solvation of nucleic acids and proteins.⁴⁵ The protocol of MD simulations applied to all six duplexes was as follows: (1) relaxation of the structure by 500 cycles of conformational energy minimization using the biconjugated gradient method, (2) slow heating of the system from the initial temperature (5 K) to room temperature (300 K) over a period of 200 ps with a 0.002 ps time step (the target temperature of the Berendsen thermostat was increased by 0.003 K for each time step), (3) equilibration of the system at a constant temperature of 300 K with a Berendsen thermostat over 500 ps, (4) a productive simulation 5 ns in length for each DNA duplex at 300 K, and (5) slow cooling of the system to 50 K over 0.5 ns to calculate the energy optimal frozen structure.

To examine an internal distortion of DNA substrate structure, the rigid root-mean-square deviation (rmsd) fit of all atoms of each snapshot to the starting conformation (B-DNA) was performed and averaged over the productive part of the MD trajectory. The respective rmsd values reflect the average deformation of the DNA substrate structure relative to B-DNA. In addition, the average DNA substrate structures were calculated over the productive MD trajectory as average positions of atoms, and then thermal fluctuations (rmsf) from the average position were calculated over the productive part of the MD trajectory for each atom of the DNA substrate. The rmsf values were estimated for each nucleotide of the duplex, indicating the amplitude of its internal mobility at 300 K, which is associated with the degree of deformability of the respective structural fragment. The molecular graphics program VMD⁴⁸ was extensively used for a visual analysis of the trajectories and for producing the figures. To assess DNA backbone kinking at the abasic site, we outlined a helix axis as an average trace made of centers of each base pair. An angle between a 5'-part (comprises bases 1–5) and a 3'-part (comprises bases 7–12) of the dodecamers was calculated after linear approximation of the

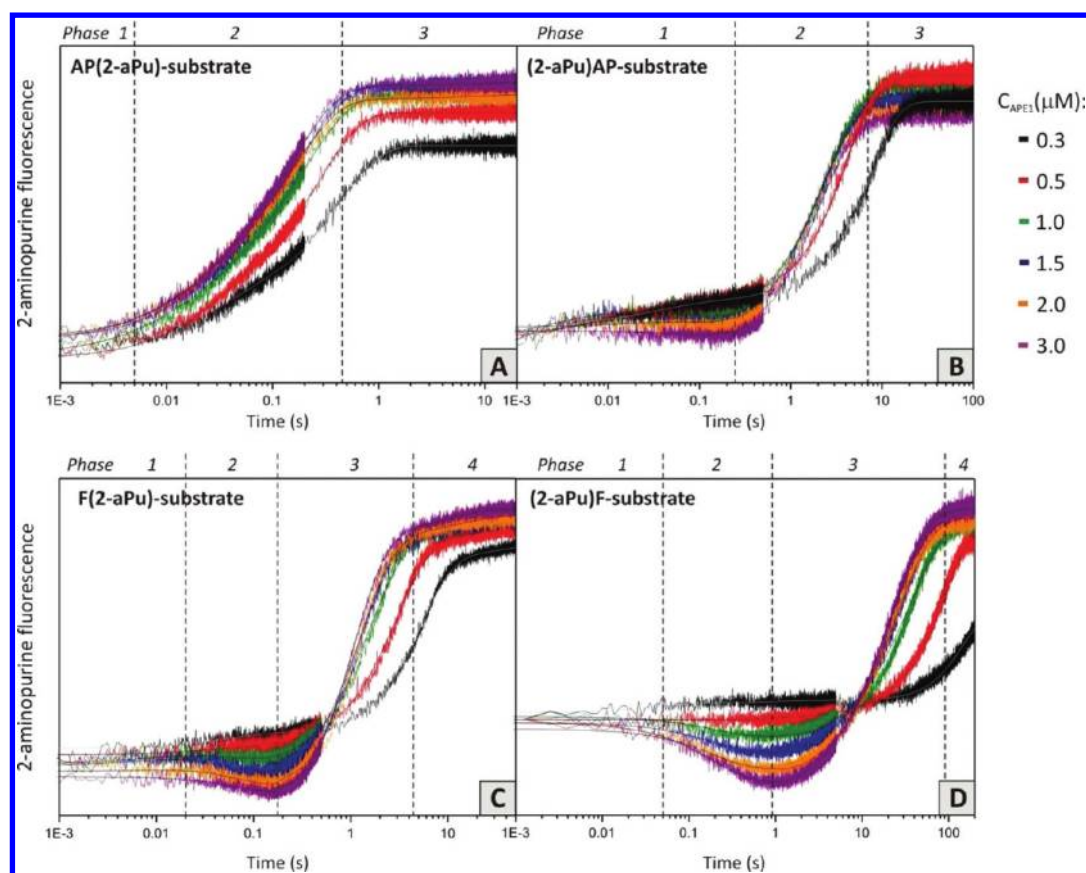


Figure 1. Stopped-flow fluorescence assays of various DNA substrates. 2-aPu fluorescence traces for interactions of APE1 with DNA substrates containing the 2-aPu residue 5' or 3' to the natural AP site (A and B) or F (C and D) are shown. The ODN concentration was 1.0 μM , and the enzyme concentrations were varied from 0.3 to 3.0 μM . Experimental data and results of global fitting are presented as jagged and smooth traces, respectively. Dashed vertical lines approximately correspond to different stages of kinetic Scheme 1.

respective axis segments. The following geometrical criterion was employed for analyzing hydrogen bonding around the site of damage: for a proton donor (D), proton (P), proton acceptor (A) system, a hydrogen bond is said to exist if the P–A distance is $<2.4 \text{ \AA}$ and the D–P–A angle is $>120^\circ$.⁴⁹

RESULTS

Stopped-Flow Assay of DNA Conformational Changes Using the 2-aPu Fluorescent Probe. To probe the conformational dynamics of damaged DNA, we applied the stopped-flow technique combined with 2-aminopurine fluorescence detection. It is known that photophysical properties of this fluorescent probe are very sensitive to the local environment and solvent polarity.^{50,51} The fluorescent signal of the 2-aPu base is quenched by hydrophobic surroundings and increases within a more hydrophilic environment.^{52,53} When inserted into DNA duplexes, the 2-aPu probe does not disturb a base stacking and was shown to form an unusually stable base pair with cytosine (wobble geometry).^{50,54} The described behavior makes 2-aPu a suitable spectroscopic probe for the detection of DNA conformational changes along the reaction pathway. Changes in the 2-aPu fluorescent signal after rapid mixing of the enzyme and DNA substrates were monitored over time. The previous study of the APE1 catalytic reaction under BER and NIR conditions with a 30-nucleotide AP-DNA performed by our colleagues revealed a high incision rate ($k_{\text{cat}}^{\text{AP}} = 12 \text{ s}^{-1}$) and the existence of a stable enzyme–product complex ($K_p = 4.8 \times 10^{-7} \text{ M}$), which precluded the

detection of individual transient complexes in the catalytic cycle.⁵⁵ Further examinations have shown that the use of shorter substrate ODNs results in decrease in the rate of its processing and, therefore, allows detection of conformational changes corresponding to steps of specific binding and incised product release.³⁷ The minimal DNA length required for efficient binding by APE1 has been determined to be 8 bp.^{16,26} The series of 12 bp 2-aPu-containing ODNs produced were thermodynamically stable (see Experimental Procedures) and did not show appreciable end effects, providing a convenient tool for detecting conformational dynamics within the nucleoprotein complex (Table 1). At first, we studied conformational transitions in ODNs carrying the fluorophore 5' or 3' to the natural abasic site. The stopped-flow analysis was performed under approximately single-turnover conditions for various concentrations of APE1 (from 0.3 to 3.0 μM) and 1 μM DNA substrates with a time interval of $\leq 100 \text{ s}$ (Figure 1A,B). A suitable observation time was optimized from preliminary stopped-flow runs when the registration of 2-aPu fluorescence was continued up to 2000 s. The resulting time courses demonstrated substantial changes in the fluorescence intensity compared with control experiments (without APE1) when the fluorescent signal kept a constant value throughout the acquisition interval (data not shown). Stopped-flow kinetic curves for AP(2-aPu) and (2-aPu)AP substrates have shown a similar increase in the magnitude of the fluorescent signal, but the time point of this change was different for them. When 2-aPu was placed 3' to the AP site within the substrate ODN, an

Table 2. Rate and Equilibrium Constants for Interactions of APE1 with Specific DNA Substrates Containing 2-Aminopurine Derived from 2-aPu and Trp Fluorescence Changes^a

	2-aminopurine fluorescence				tryptophan fluorescence			
	AP(2-aPu)	(2-aPu)AP	F(2-aPu)	(2-aPu)F	AP(2-aPu)	(2-aPu)AP	F(2-aPu)	(2-aPu)F
k_1 (M ⁻¹ s ⁻¹)	4.8×10^7	2.6×10^6	1.9×10^7	3.5×10^6	2.1×10^8	1.0×10^7	1.2×10^7	1.9×10^7
k_{-1} (s ⁻¹)	3.1	7.0	38	11	54	61	47	77
k_2 (s ⁻¹)			7.5	1.3		9.3	12	13
k_{-2} (s ⁻¹)			2.1	0.56		1.1	0.71	1.9
k_{incision} (s ⁻¹)	7.1	0.50	1.5	0.08	5.7	0.37	2.8	0.08
K_D (M)	2.0×10^{-7}	1.9×10^{-6}	1.1×10^{-6}	3.8×10^{-6}	1×10^{-6}	4.2×10^{-6}	7.5×10^{-7}	4.1×10^{-6}
K_a (M ⁻¹) ^b	1.6×10^7	3.7×10^6	2.2×10^6	1.1×10^6	3.8×10^6	1.5×10^6	4.6×10^6	1.9×10^6

^aThe standard error of the presented values of rate constants was within 30%. ^bEquilibrium association constant K_a was calculated with the equation $K_a = \sum_{i=1}^N \prod_{j=1}^i K_j$ for N -step binding (see Scheme 1). $K_j = K_j/k_{-j}$.

appreciable elevation of the fluorescence intensity was observed from 5 ms to 0.45 s (see phase 2 in Figure 1A). In the case of the (2-aPu)AP substrate, the described fluorescence change was shifted to larger values of the time scale (0.25–7 s) (see phase 2 in Figure 1B). To associate detected conformational transitions with particular steps of the APE1 catalytic cycle, we should take into account the fluorescence properties of the 2-aPu probe described above. Indeed, the irreversible step of substrate cleavage leads to the formation of shorter oligonucleotides carrying the 2-aPu base at the 5' or 3' end. This process should result in an increase in the fluorescence intensity due to the transition of 2-aPu to a more hydrophilic environment. To elucidate the reaction mechanism, we visually inspected stopped-flow kinetic curves; the traces were divided into several phases (dashed vertical lines in Figure 1A,B), consistent with changes of the slope of tangents to the trace. Each phase represents a characteristic time of particular transient states of the DNA substrate arising throughout the catalytic cycle. For both AP(2-aPu) and (2-aPu)AP substrates, a slow change in fluorescence intensity in the first phase most likely displayed the substrate binding step. The second phase of the curves corresponded to a sharp increase in fluorescence intensity, indicating DNA cleavage followed by release of product ODNs from the active site in the third phase. The obtained stopped-flow data have been kinetically described by a three-step mechanism that includes two transient enzyme–DNA complexes (Scheme 1). To extract individual rate constants, we directly fit fluorescence traces by treating the corrected fluorescence intensity as the sum of the contribution of each fluorescent DNA species at any reaction time as described previously.³⁷ Kinetic parameters obtained from the numerical fitting are listed in Table 2 (see the 2-aminopurine fluorescence columns). The quality of the fit was estimated by visual comparison of overlays of the fitted curves and experimental data as well as by inspection of the residuals (Figure S1 of the Supporting Information). Errors in the determined constants consisted of instrumental errors and the standard error arising during the use of a nonlinear least-squares regression algorithm. The resultant error values were around 30%. A detailed analysis of kinetic parameters has revealed that both substrates formed a stable complex with APE1, which follows from the calculated values of equilibrium constant K_a of 1.6×10^7 and 3.7×10^6 M⁻¹ for AP(2-aPu) and (2-aPu)AP substrates, respectively. On the other hand, the rate constant of the irreversible cleavage step (k_{incision}) was 7.1 s⁻¹ for the AP(2-aPu) substrate and only 0.5 s⁻¹ for another one, indicating a 14-fold decrease in the reaction rate when the location of the 2-aPu base is changed from the 3' end to the 5' end of the AP site.

Determination of a unique solution to the kinetic model during global analysis of complex kinetic schemes is a difficult problem. The smooth shapes of fluorescence curves without extreme points at short times do not allow us to determine exactly the values of the reverse rate constants for early steps. It is possible to say with confidence that equilibrium constants and incision step kinetic constants are reliably determined. In the assignment of the kinetic transients to different stages of the enzymatic process, we take into account all the data, including the fluorescence curve fitting, the data from PAGE separation of products, and the equilibrium fluorescence titration.

Next, we examined the conformational dynamics of DNA substrates containing 2-aPu residues adjacent to the tetrahydrofuran (F). F is a synthetic AP site analogue lacking the C1'-hydroxyl group that is normally recognized and processed by human APE1. DNA substrates containing the F moiety as a lesion have been widely used for studying DNA repair enzymes.^{26,44,56–58} In our recent paper, we applied this stable lesion analogue for the pre-steady-state kinetic analysis of its interactions with APE1.³⁷ Here we employ ODNs containing the F moiety flanked by 2-aPu as specific substrates for APE1 to investigate the DNA dynamics in detail (Table 2). Stopped-flow kinetic curves for different concentrations of the enzyme (0.3–3 μM) were collected by monitoring the 2-aPu fluorescence over time (Figure 1C,D). In both cases, the resulting curves showed two types of fluorescence changes: a fast and decreasing phase followed by a slow and increasing phase. The stopped-flow traces of F-containing DNA substrates were analyzed as described above and displayed an additional conformational transition before the incision step that was absent in the case of the natural AP site. As follows from Figure 1, conformational transitions of F(2-aPu) and (2-aPu)F substrates include four phases. The first phase corresponds to initial binding and formation of the primary enzyme–substrate (ES) complex. The next phase is the 2-aPu fluorescence decay that represents further adjustment of the DNA structure for catalysis and results in the appearance of catalytically active complex (ES1). The third and fourth phases are characterized by high-amplitude growth followed by a steady level of fluorescence intensity associated with the accumulation of the product and its release. It can clearly be seen that the process of F(2-aPu) substrate cleavage was essentially complete after 10 s, whereas in the case of the (2-aPu)F substrate, it required more than 100 s. The quantitative analysis of fluorescence traces allowed us to propose a four-step kinetic mechanism for these reactions (Scheme 1) and to determine rate constants for each step of the scheme (Table 2, third and fourth columns from the left). The observed influence of the location of 2-aPu on the

APE1 reaction rate was confirmed by calculated values of the catalytic k_{incision} constant of 1.5 and 0.08 s⁻¹ for F(2-aPu) and (2-aPu)F substrates, respectively. This observation is in good agreement with the stopped-flow data for AP(2-aPu) and (2-aPu)AP substrates. Upon comparison of the rates of incision of AP- and F-containing DNA, we have found an evident preference for the natural abasic site expressed as a 6-fold decrease in the k_{incision} value. In support of this observation, calculated values of the equilibrium association constant (K_a) are 2.2×10^6 and 1.1×10^6 M⁻¹ for F(2-aPu) and (2-aPu)F substrates, respectively, suggesting a lower affinity of the APE1 for the synthetic abasic site analogue as compared to that of the natural AP site. The last equilibrium step of the kinetic scheme is a reversible dissociation of cleaved DNA products from APE1 described by the K_D constant. Depending on the substrate type, K_D values determined in stopped-flow experiments indicate the existence of a more or less stable (EP) complex. To summarize, we found that the cleavage rate is significantly reduced when the normal cytosine of AP and F substrates is substituted with 2-aPu 5' to the abasic site (see Table 5). By contrast, the 3' 2-aPu either has no effect on the substrate processing or can even facilitate APE1 catalysis. This further confirmed that the upstream DNA region relative to the site of damage is important for the right coordination of binding and incision steps of the catalytic reaction.

Direct PAGE Analysis of the Accumulation of Nicked Products. To associate conformational transitions detected in the stopped-flow fluorescence assay with particular chemical steps of the APE1 catalytic cycle, we performed a denaturing PAGE analysis of the accumulation of reaction products. In this assay, substrate ODNs were labeled with ³²P and then mixed with the APE1 under conditions similar to those of stopped-flow experiments. Autoradiograms obtained for each substrate type are available as Supporting Information (Figure S2). The respective time courses, presented in Figure 2, demonstrated a

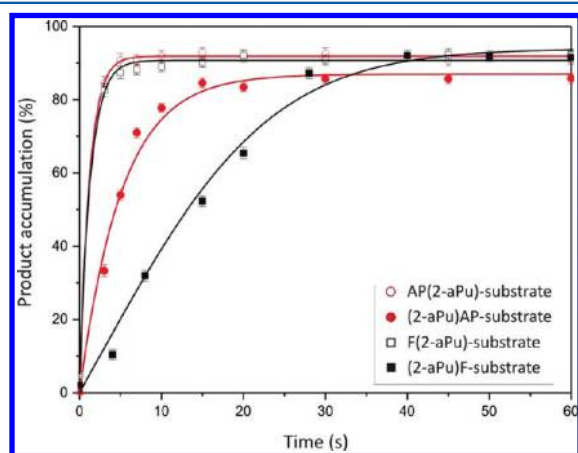


Figure 2. Cleavage of ³²P-labeled 2-aPu-containing DNA substrates by APE1. Time courses of accumulation of the cleaved product for all substrate types are shown. Reaction mixtures (10 μ L) contained 1.5 μ M substrate and 1.5 μ M enzyme. Error bars reflect the standard error of the mean from three independent experiments.

rapid accumulation of the incised products. The appearance of bands that corresponded to the product ODNs for all substrates occurred over the same time interval that we proposed from the stopped-flow fluorescence measurements. Indeed, AP(2-aPu) and F(2-aPu) substrates exhibited the highest incision rate and were converted into the product

within 3 s. The minimal reaction time point on the autoradiograms was limited by the capabilities of the applied technique. Accordingly, the (2-aPu)F substrate was the slowest; accumulation of approximately 80% of the product required more than 30 s. The results of the chemical quench assay evidently confirm that the sharp increase in 2-aPu fluorescence observed in the stopped-flow traces corresponds to the irreversible cleavage step (k_{incision}) of the proposed Scheme 1.

Pre-Steady-State Stopped-Flow Assay of APE1 Conformational Dynamics. To gain extensive knowledge of the APE1 kinetic mechanism, we conducted the stopped-flow assays with 2-aPu-containing DNA substrates combined with detection of the Trp fluorescence intensity of the enzyme. The time courses of fluorescence changes of 1.5 μ M APE1 were registered at an increasing DNA concentration (0.5–4 μ M) under approximately single-turnover conditions (Figure 3A–D). Multiple conformational transitions were observed on fluorescence traces of each of the concentration series, indicating that the enzyme undergoes more complex conformational changes than DNA substrates. To begin, we examined possible transient states of the APE1 molecule under AP(2-aPu) substrate processing, which are reflected in changes in the slope of tangents to the trace (Figure 3A). Similar to analysis of the 2-aPu fluorescence traces, the kinetic curves on Trp fluorescence were divided into several phases marked with dashed vertical lines in Figure 3. The first phase of the rapid decrease in the Trp fluorescence intensity observed up to 9 ms is associated with substrate binding and formation of the primary enzyme–substrate complex (ES). The subsequent growth of the fluorescence signal from 0.01 to 0.4 s most likely corresponds to the irreversible incision step that resulted in formation of (EP). Described conformational transitions eventually led to the release of the incised DNA product (P) from the active site at the same time with the establishment of a constant value of fluorescence intensity. The minimal kinetic scheme satisfying experimental data has been determined by the global fitting and has included two transient states of APE1 (Scheme 1). The values for the individual rate constants are summarized in Table 2 (see the tryptophan fluorescence columns). The bimolecular encounter between the enzyme and AP(2-aPu) substrate is described by the forward and reverse rate constants of 2.1×10^8 M⁻¹ s⁻¹ and 54 s⁻¹, respectively, which are typical for this process. The calculated equilibrium association constant K_a for this interaction is 3.8×10^6 M⁻¹, corroborating the rather good affinity of APE1 for this type of DNA substrate. The value of the constant for the irreversible step for the AP(2-aPu) substrate ($k_{\text{incision}}^{\text{Trp}} = 5.7$ s⁻¹) is in good agreement with the rate constant derived from 2-aPu fluorescence measurements ($k_{\text{incision}}^{2\text{-aPu}} = 7.1$ s⁻¹). The difference in the values of the rate constants of equilibrium steps, derived from 2-aPu and Trp fluorescence curves, may be connected with the different physical processes detected in these cases.

When studying the pre-steady-state kinetics of (2-aPu)AP substrate cleavage, we observed an additional conformational transition in the protein molecule on Trp fluorescence curves within 0.04–0.3 s (Figure 3B). This bend took place upon APE1–DNA binding, and mutual adjustment was absent on the Trp fluorescence traces of AP(2-aPu) substrate processing. Notably, with a similar shape of their fluorescence curves, these DNA substrates were processed by APE1 with greatly different rates. A distinct rise in the Trp fluorescence between 0.3 and 7 s represented the step of catalytic incision described by a k_{incision}

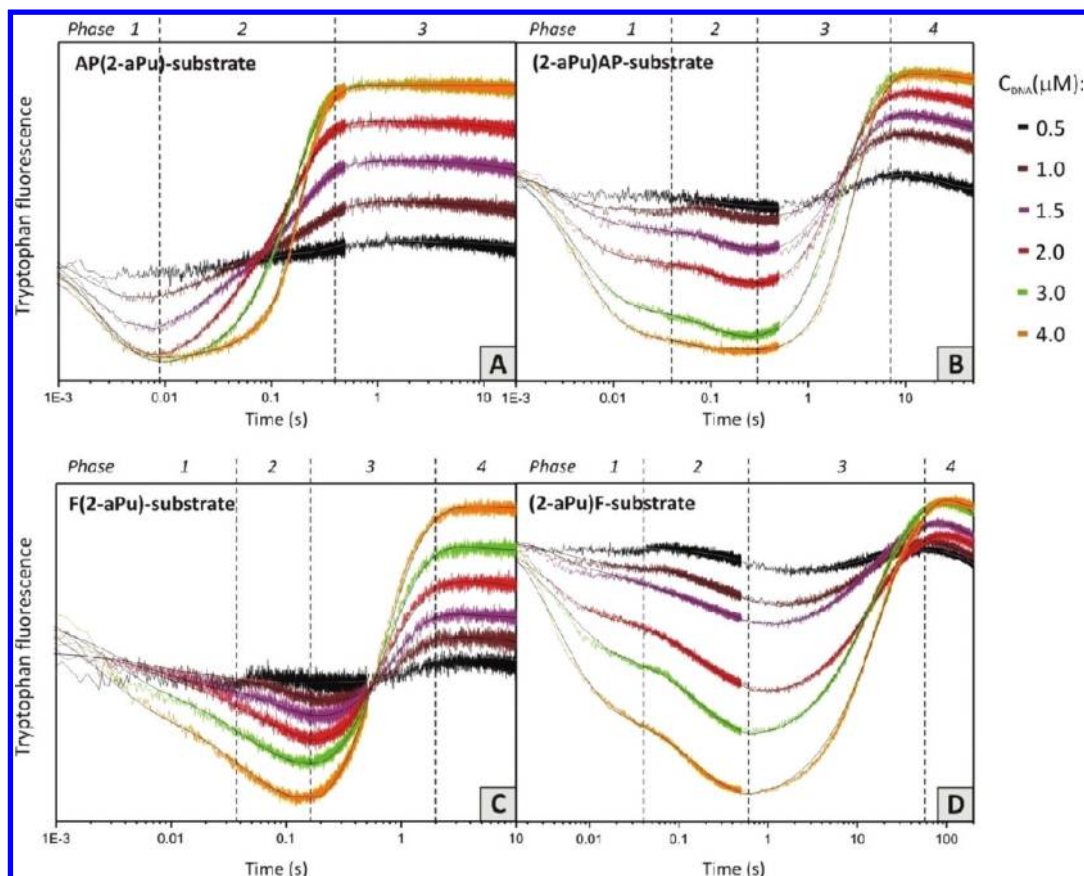


Figure 3. Stopped-flow Trp fluorescence traces for interactions of APE1 with DNA substrates containing the 2-aPu residue 5' or 3' to the natural AP site (A and B) or F (C and D). The APE1 concentration was 1.5 μM , and the ODN concentrations were varied from 0.5 to 4.0 μM . Experimental data and results of global fitting are presented as jagged and smooth traces, respectively. Dashed vertical lines approximately correspond to different stages of kinetic Scheme 1.

value of 0.37 s^{-1} . The quantitative analysis of experimental data yielded a four-step reaction mechanism, including two different precatalytic complexes (ES and ES1) (Scheme 1). Comparison of cleavage rates for AP(2-aPu) and (2-aPu)AP substrates reported by 2-aPu and Trp fluorescence reveals the same dependence. Displacement of the 2-aPu base from upstream to downstream of the AP site results in a 15-fold decrease in k_{incision} . Thus, our stopped-flow data for different fluorophores evidently support each other, facilitating elucidation of individual events of the APE1 catalytic cycle.

At the next stage of the study, we followed the dynamics of the APE1 conformation during interactions with F(2-aPu) and (2-aPu)F substrates. Two series of stopped-flow traces were collected at increasing concentrations of DNA duplexes (0.5–4 μM) in the time interval up to 200 s. The results of the experiments are illustrated in panels C and D of Figure 3. The fluorescent curves have a common shape, resembling kinetic curves for the AP-containing substrates examined above (Figure 3A,B). As expected, a slight bend associated with the additional conformational transition of APE1 before the incision step was also observed in the second phase (Figure 3C). On the basis of the global fitting results, we have proposed a kinetic mechanism consisting of three transient states of the enzyme (Scheme 1). The third phase of the curves corresponding to the catalytic incision step was characterized by the lowest rate constants of 2.8 and 0.08 s^{-1} for F(2-aPu) and (2-aPu)F substrates, respectively. Therefore, the tendency of the reaction rate to be reduced depending on the location of the 2-aPu probe was

also found for F-containing substrates. Comparison of the 2-aPu and Trp fluorescence traces for each DNA substrate has shown that conformational transitions of the enzyme and DNA molecules occurred over the same time intervals. In particular, during interactions of APE1 and the (2-aPu)F substrate, time courses of both fluorophores demonstrate a biphasic fluorescence decay up to 1 s that involves two precatalytic steps of the mechanism that result in (ES) and (ES1) complexes (Figures 1D and 3D). Close examination of initial segments of the traces suggests that the second fluorescently discernible phase on Trp kinetic curves ($\sim 0.08\text{ s}$) gives rise to the conformational change in DNA structure within 0.1–0.5 s. The subsequent third and fourth phases that resulted in product formation and release also coincide on a time scale for both fluorophores. Another finding from Trp fluorescence detection is that the fluorescence level of the last phase of the kinetic curves attributed to completion of the reaction and release of APE1 seems to be much higher than the initial fluorescence value. These levels were nearly the same only for processing of the slowest (2-aPu)F substrate. This is probably because of the high rate of enzyme turnover observed during incision of AP(2-aPu), F(2-aPu), and (2-aPu)AP substrates, when formation of the collisional complex is too fast to detect the appropriate enzyme fluorescence changes by the stopped-flow method.

Analysis of the Affinity of APE1 for Product ODNs. The affinity of APE1 for the reaction product was analyzed by fluorescence titration of the enzyme with an equimolar mixture

of three oligonucleotides representing the products of F(2-aPu) and (2-aPu)F substrate cleavage (Table 3). Under conditions

Table 3. Sequences of ODNs Used in Fluorescence Titration Experiments Representing the Products of Substrate Cleavage by APE1

name	product structure	K_D^{titr} (M) ^a
P1	5' d(CTCTC) 3' 5' d(pF(2-aPu)CTTCC) 3' 5' d(GGAAGCCGAGAG) 3'	$(3.7 \pm 0.5) \times 10^{-6}$
P2	5' d(CTCT(2-aPu)) 3' 5' d(pFCCTTCC) 3' 5' d(GGAAGCCGAG) 3'	$(3.3 \pm 0.4) \times 10^{-6}$

^a K_D^{titr} represents an equilibrium dissociation constant extracted from fitting of experimental points to a one-site binding model (Figure 4).

used in our experiments, such short ODNs ($n = 5$ or 6) cannot form stable duplexes in solution. However, in the presence of the enzyme, these end product oligonucleotides are stabilized in the duplex form bound to APE1. We conducted these experiments to estimate the stability of the APE1–product complex expressed by the last equilibrium of the kinetic scheme by an independent method. Figure 4 demonstrates changes in

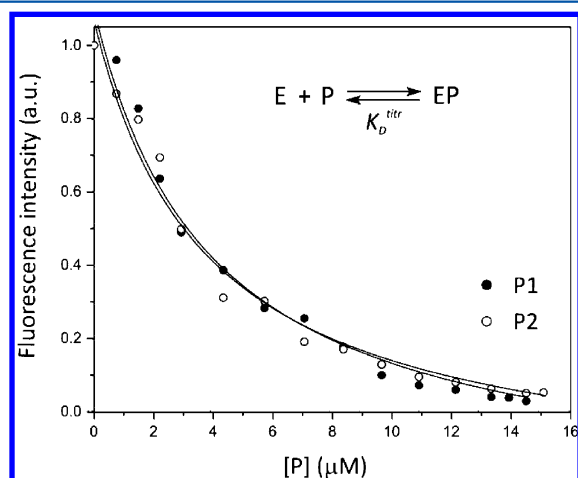


Figure 4. Change in the Trp fluorescence signal during titration with oligonucleotides corresponding to products P1 and P2 of F(2-aPu) and (2-aPu)F substrate cleavage, respectively (see also Table 3). A simple one-step binding scheme is characterized by the equilibrium dissociation constant K_D^{titr} . Structures of P1 and P2 as well as the values of the constant are listed in Table 3. [P] is the concentration of the oligonucleotides.

the fluorescence intensity of the enzyme during titration with both types of DNA products. The data were fit to a one-site binding model described by an equilibrium constant K_D^{titr} (Figure 4 and Table 3). The calculated values of K_D^{titr} for products P1 and P2 were $(3.7 \pm 0.5) \times 10^{-6}$ and $(3.3 \pm 0.4) \times 10^{-6}$ M, respectively, indicating the formation of a stable complex between the protein and nicked 2-aPu-containing DNA. Taking into account the minor difference in the constant values, we found the stability of the EP complex should be considered comparable for P1 and P2. This observation is in general agreement with the values of K_D obtained from stopped-flow data for both fluorophores. Comparison of the determined K_D^{titr} values for 2-aPu-containing products with recently reported data³⁷ has revealed a >1 order of magnitude

decrease in the stability of the EP complex after introduction of the 2-aPu base into DNA adjacent to the site of damage.

MD Simulations of DNA Substrate Structure. To understand the observed sequence context effect, we performed independent MD simulations for six DNA substrates. As a result of MD trajectories, an optimized three-dimensional structure of each 2-aPu-containing DNA along with distinguishing structural parameters has been obtained (Figure 5A–D). It should be noted that the average structure coincided with the energy optimal structure with an rmsd of ~ 0.1 Å. To estimate the deviation of damaged DNA duplexes from canonical B-DNA, we determined the rmsd values and bending of DNA helices in all simulations (Table 4). Another suitable parameter used for comparison of the substrates was the value of thermal fluctuation (rmsf) that describes the extent of internal movement of the duplex bases and its structural deformability (Table 5). At first, AP and F substrates without the 2-aPu probe were studied, yielding rmsd values that converged to 2.8 and 3.1 Å, respectively. Additionally, the AP or F site introduced into 12 bp DNA induces kinking at the abasic site of $\sim 37^\circ$ or 42° , respectively. In the case of AP substrate modeling, we have observed a non-Watson–Crick hydrogen bond between the hydroxyl (OH) group of abasic ribose and O2 of the neighboring C₅ (1.99 Å) (data not shown). The findings that are in good agreement with previously reported data^{49,59} were subsequently used to assess the structural diversity of 2-aPu-containing ODNs. In Figure 5, we present views of four 2-aPu-containing duplexes extracted from computer modeling. The energy-optimized structures demonstrate a significant deviation from both canonical B-DNA and AP or F substrate structures; albeit, it generally occurs near the abasic site. It should be noted that in all simulations the 2-aPu–C mispair was in a wobble geometry stabilized by two hydrogen bonds.⁶⁰ The smallest degree of DNA helix distortion has been found for the AP(2-aPu) substrate simulation, resulting in an rmsd of ~ 1.9 Å and a helix kink of $\sim 15^\circ$ (Figure 5A and Table 4). For this structure, we also observed two hydrogen bonds in the region of the abasic sugar, not apparent for the AP substrate. The first one involved amino protons of C₁₉ and the OH group of the AP site (2.17 Å), and the second involved O2 of C₁₉ and amino protons of 2-aPu₇ (2.12 Å). At the same time, as follows from rmsf values (~ 1.1 Å), the AP(2-aPu) substrate structure is the most flexible among DNA substrate duplexes studied (Table 5). Furthermore, our experimental observations suggest the AP(2-aPu) substrate ($k_{\text{incision}}^{\text{SF}} \sim 6$ s^{−1}) is a better candidate for specific recognition and cleavage by APE1 than other 2-aPu-containing ODNs or the AP substrate ($k_{\text{incision}}^{\text{SF}} = 3.2$ s^{−1}), as well.

During the simulation of the (2-aPu)AP substrate, a substantial bending of the sugar–phosphate backbone into the major groove was found (Figure 5B). The resulting average structure shows kinking at an angle of $\sim 63^\circ$ between the 5' and 3' parts of the duplex accompanied by compression of the abasic site void opposite the orphan C₁₉ base. The rmsf values for nucleotides of the (2-aPu)AP duplex demonstrate a lower conformational flexibility relative to those of the DNA substrates mentioned above (the overall rmsf values are presented in Table S1 of the Supporting Information). At the same time, the 2-aPu₅–C₂₀ base pair approaches the AP site through hydrogen bonding (2.18 Å) and, thereby, stabilizes the specific orientation of the abasic sugar ring rotated by an angle of $\sim 90^\circ$. The observed strong deformation of the (2-aPu)AP substrate helix (rmsd = 4.5 Å) coupled with its low mobility

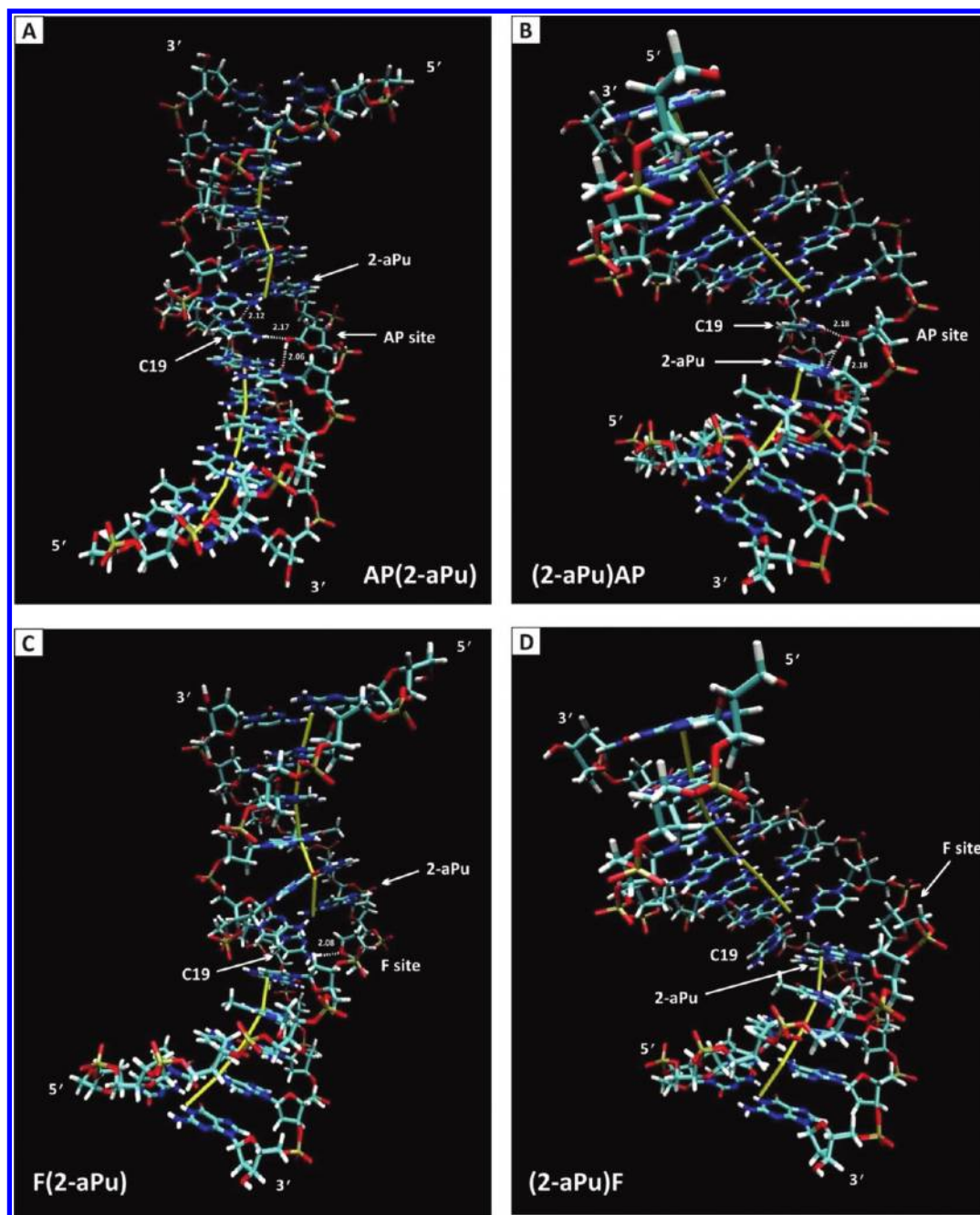


Figure 5. Stereoviews of the average structure of the AP(2-aPu) substrate (A), (2-aPu)AP substrate (B), F(2-aPu) substrate (C), and (2-aPu)F substrate (D). The global helix traces are superimposed (yellow). The locations of the abasic sugar (AP or F), the 2-aPu probe, and the orphan pyrimidine are indicated for each duplex. Non-Watson–Crick hydrogen bonds are shown as white dotted lines. The numbers represent the H-bond lengths (angstroms).

Table 4. Quantitative Parameters of Different Abasic DNA Distortion Relative to Canonical B-DNA Obtained from MD Simulations

duplex name	DNA kink angle (deg)	rmsd (Å)
AP substrate	36.9	2.82
F substrate	41.8	3.11
AP(2-aPu) substrate	15.2	1.93
F(2-aPu) substrate	44.9	3.30
(2-aPu)AP substrate	63.2	4.47
(2-aPu)F substrate	60.6	4.35

(rmsf ~ 0.26 Å) seems to complicate the capture of the extrahelical AP site by Trp²⁸⁰, Phe²⁶⁶, and Leu²⁸² of APE1, resulting in a reduced rate of catalysis ($k_{\text{incision}}^{\text{SF}} = 0.5 \text{ s}^{-1}$).

By comparing the simulation of the F(2-aPu) substrate versus the F substrate, we have found its sugar–phosphate backbones to be inherently consistent, except for the region from A₁₆ to C₁₉ of the complementary strand that is displaced toward the DNA major groove (Figure 5C). This structural fluctuation results in the helix axis kinking adjacent to F ($\sim 45^\circ$) and gives rise to a change in the helix geometry parameters, including the inclination (2-aPu₇·C₁₈, C₈·G₁₇, and T₇·A₁₆ base pairs), propeller twist (2-aPu₇·C₁₈), and buckle (C₅·G₂₀ and

Table 5. Thermal rmsf Values for Individual Nucleotides Adjacent to the Abasic Site^a

nucleotide	AP	F	AP(2-aPu)	F(2-aPu)	(2-aPu)AP	(2-aPu)F
strand 1						
5	0.37	0.26	1.29	0.26	0.26	0.49
6 (AP/F site)	0.44	0.35	1.06	0.26	0.26	0.60
7	0.46	0.27	1.13^b	0.23	0.26	0.43
strand 2						
18	0.80	0.25	0.54	0.24	0.37	0.34
19 (orphan C)	0.49	0.37	0.44	0.25	0.27	0.42
20	0.32	0.25	0.46	0.29	0.25	0.42
k_r^{SF} (s ⁻¹) ^c	3.2	2.1	7.1	1.5	0.5	0.08

^aThe values (angstroms) for the central 3 bp of the damaged (strand 1) and complementary (strand 2) strands are shown. A full list of rmsf values is provided in Table S1 of the Supporting Information. ^brmsf values for 2-aminopurine nucleotides are given in bold. ^cThe values of k_r^{SF} were taken from stopped-flow kinetic data and represent the rate of cleavage of the DNA substrate by APE1. The experimental and modeling data indicate the following order of AP- or F-containing substrate preference by APE1: AP(2-aPu) > AP > (2-aPu)AP; F > F(2-aPu) > (2-aPu)F.

C₈·G₁₇). There is also a hydrogen bond between O4' of the abasic sugar and amino protons of C₁₉ (2.08 Å). According to the rmsf values (~0.26 Å), the F(2-aPu) substrate structure is more or less stable, displaying low conformational dynamics. Because of enhanced stacking and hydrophobic interactions between neighboring nucleotides around the opposite C₁₉ base, the important DNA recognition elements become less accessible, while the target F site retains an unkinked conformation (as compared to the F substrate). Supporting this hypothesis, our stopped-flow data indicate that the reduced rate of F(2-aPu) substrate processing occurs presumably at steps of specific binding and precatalytic complex formation rather than at the incision step ($k_{incision}^{SF} = 1.5 \text{ s}^{-1}$).

MD simulations have shown a dramatic DNA distortion (rmsd = 4.4 Å), when 2-aPu is a 5' neighbor of the F site (Figure S5D). The "top" part of (2-aPu)F substrate helix (consisting of nucleotides C₁₁, C₁₂, G₁₃, G₁₄, etc.) appears to be deflected at an angle of ~60° with respect to the "bottom" part. No hydrogen bonding was observed between the F ring and neighboring bases. Moreover, the abasic site void of the average structure is strongly compressed so that the opposite C₁₉ is expelled from the helix with no ability to fluctuate (rmsf = 0.42 Å). Overall, the bottom part of the structure (consisting of base pairs 2-aPu·C₂₀, T₄·A₂₁, etc.) exhibits rather large perturbations versus the top part, involving unusual roll, tilt, and buckle angles. It is important that in conformity with pre-steady-state kinetic data the (2-aPu)F substrate is the worst for endonuclease reaction among the ODNs studied, having a significantly reduced rate of formation of the specific APE1–DNA complex and catalytic incision ($k_{incision}^{SF} = 0.08 \text{ s}^{-1}$).

DISCUSSION

In our recent work, the pre-steady-state kinetics of abasic site repair by human APE1 was studied.³⁷ The stopped-flow approach in combination with Trp fluorescence detection has revealed the conformational mobility of the enzyme in the course of recognition and catalytic incision of AP- or F-containing DNA. On the basis of the enzyme fluorescence changes over time, the APE1 molecule was shown to undergo at least four conformational transitions along the reaction coordinate. Kinetic parameters determined in stopped-flow experiments are suggestive of a very high processing rate for 12-mer abasic DNA ($k_{cat} \sim 3 \text{ s}^{-1}$). Our findings have also shown a meaningful difference in rates of reaction between AP and F substrates, indicating the C1'-hydroxyl moiety of the abasic

sugar to be essential for effective recognition and catalysis. Although the stopped-flow data obtained for Trp fluorescence provided new critical information about the APE1 catalytic reaction, clarification of the nature of the observed transient states required further examination.

2-aPu Fluorescence Reveals Conformational Transitions within the DNA Helix during Interactions with Human APE1.

To achieve the goal of this study, we incorporated the 2-aPu nucleoside into 12-mer ODNs 5' or 3' to the natural AP site or F to serve as an on-site reporter of interactions of APE1 with the site of damage. Under single-turnover conditions, the process of incision of abasic DNA by APE1 was studied by monitoring of the 2-aPu fluorescence changes over time. To identify the reaction mechanism and extract kinetic parameters, we obtained fluorescence traces for the series of APE1 concentrations, whereas the concentration of DNA was 1 μM in all experiments. It is interesting to note that nonspecific binding of APE1 to the undamaged 2-aPu-containing duplex was not accompanied by 2-aPu fluorescence changes, except for a very small increase in the fluorescence signal within 0.05 s (Figure S3 of the Supporting Information). The observed conformational change in all likelihood represents a local destabilization of DNA base stacking as a result of the primary nonspecific complex formation. Fitting the experimental curves to a one-site binding model has shown a low affinity of APE1 for the normal 2-aPu-containing DNA ($K_a = 1.9 \times 10^5 \text{ M}^{-1}$). A completely different situation was observed in 2-aPu fluorescent traces in the case of specific substrate cleavage. As shown in Figure 1, interactions of APE1 with the abasic site led to substantial conformational changes in substrate molecules corresponding to the enzyme binding and cleavage steps. The kinetic curves for AP(2-aPu) and (2-aPu)AP substrates demonstrate two phases of fluorescence changes (Figure 1A,B), whereas substitution of the natural AP site with F enlarges the number of fluorescently discernible phases to three (Figure 1C,D), regardless of the location of the 2-aPu probe. Considering that the fluorescence properties of 2-aPu depend generally on stacking interactions and solvent polarity, we suggest that the fast and slight decrease in fluorescence intensity observed for F(2-aPu) and (2-aPu)F substrates (0.02–1 s time interval) reflects a kind of DNA conformational transition resulting in a more buried transient state of the abasic site. The more pronounced and slow increase in the 2-aPu fluorescence that occurred for all substrates most likely corresponds to translocation of the fluorophore from the

hydrophobic pocket of APE1 to the polar solvent environment. To explore what phase of 2-aPu fluorescent traces reflects directly the step of DNA cleavage, the chemical quench assay of incision of ^{32}P -labeled substrates was performed (Figure 2). The time courses obtained from PAGE analysis demonstrate rapid accumulation of short incised ODNs that coincided on the time scale with the phase of 2-aPu fluorescence growing on the stopped-flow traces. Thus, the results obtained by independent methods evidently confirm that the noticeable growth of the 2-aPu fluorescence signal on the kinetic curves corresponds to the release of incised oligonucleotide products from the enzyme active site.

A visual inspection of fluorescence traces followed by the quantitative analysis provided a minimal kinetic mechanism for each DNA substrate (Scheme 1) as well as kinetic parameters describing the individual steps (Table 2). The fluorescence traces of stopped-flow series were divided into several phases according to the number of individual steps in the appropriate kinetic scheme. Thus, measurements of 2-aPu fluorescence changes in real time have revealed two transient states for AP-containing DNA substrates and three transient states in the case of F-containing substrates because of the additional conformational change before catalysis (phase 2 in Figure 1C,D). The values of the irreversible step constant (k_{incision}) demonstrate a significant dissimilarity in rates of catalysis between different ODNs. Indeed, the highest incision rate has been observed for the AP(2-aPu) substrate (7.1 s^{-1}), and the slowest one has been shown for the (2-aPu)F substrate (0.08 s^{-1}). This effect may probably be due to structural difficulties arising during formation of the catalytically active complex when it interacts with the F(2-aPu) or (2-aPu)F substrate, which, in turn, shifts the reaction completion to longer times. Therefore, as follows from 2-aPu fluorescence data, there are two independent factors that definitely reduce the rate of APE1 catalysis. First, substitution of the natural AP site with the chemically stable F site leads to a 6-fold decrease in the processing rate (in terms of k_{incision}). Second, when 2-aPu is a 5' abasic site neighbor, a 15–20-fold decrease in APE1 efficiency has been found. As a result of the findings, two questions were addressed: the nature of the conformational transition observed for F(2-aPu) and (2-aPu)F substrates before the cleavage step and how the location of the 2-aPu probe may influence the reaction rate. The probable answers will be discussed below, with the help of the APE1 conformational dynamics and MD simulations.

Conformational Dynamics of the Enzyme Contributes to the Interpretation of Discovered Transient States of the APE1–DNA Complex. To further understand the nature of DNA conformational changes, we followed the protein dynamics during interactions with 2-aPu-containing substrates. In stopped-flow assays, the Trp fluorescence signal was excited and monitored separately from 2-aPu fluorescence. The series of time dependencies demonstrate a conformational mobility of APE1 during processing of the ODNs (Figure 3). On the basis of qualitative and quantitative analyses, the four-step kinetic mechanism was proposed for all ODN types, except for the AP(2-aPu) substrate described by the three-step mechanism, according to Scheme 1. The kinetic curves, with few exceptions, have the same overall shape, while the time of appearance of specific conformational changes varies between different substrates. A rapid decrease in the fluorescence intensity in the first phase of the curves is associated with binding of APE1 to the target site, resulting in a stable primary (ES) complex. For most of the substrates, the process of DNA binding and the

transition into the catalytically active complex (ES1) is accomplished in two steps, including the additional step of slight growth of the Trp fluorescence en route to a minimum of the traces (phase 2 in Figure 3B–D). In the third and fourth phases of the curves, the enzyme fluorescence increased substantially and then remained unchanged, reflecting the APE1 conformational changes that corresponded to formation of the reaction product and release. Monitoring the protein dynamics has revealed a completely identical influence of the abasic ring nature and location of the 2-aPu probe on the reaction rate as found for DNA dynamics. In particular, the AP(2-aPu) substrate is the best candidate for cleavage by APE1 with a k_{incision} value of 5.7 s^{-1} , and the (2-aPu)F substrate is the worst, characterized by the slowest incision rate (0.08 s^{-1}).

According to calculated kinetic parameters, the rate of APE1 catalysis depends on the substrate structure and decreases in the following order: AP(2-aPu) > F(2-aPu) \geq (2-aPu)AP > (2-aPu)F. The first outcome of the dependence is a reduction in the cleavage rate after the natural AP site had been substituted with F. It should be noted that this observation agrees well with our previous stopped-flow results for Trp fluorescence.³⁷ The preference for the natural AP site can be explained with the help of structural considerations. In contrast to the saturated and chemically resistant ring of the F site, the AP site exists as an equilibrium mixture of hemiacetal enantiomers and hydrated aldehyde forms,⁶¹ which are specifically recognized by amino acids of the APE1 active site. Specifically, the hydrophobic pocket of Phe²⁶⁶, Trp²⁸⁰, and Leu²⁸² is considered to stabilize an extrahelical abasic site.¹⁶ In addition, a recently published report suggests that the side chain of conserved Asn²¹² interacts with the AP site via H-bonds to the 5'-phosphate or sugar oxygens, facilitating incision of the substrate.⁶² Thus, it seems very probable that the decreased reaction rate in the case of F(2-aPu) and (2-aPu)F substrates is associated with the weakened ability of the enzyme to properly orient the target site for catalysis.

To clarify the possible factors leading to the observed sequence context effect, we applied a computer modeling to all DNA duplexes studied. As a result of MD simulations, we found that DNA substrates containing the 2-aPu base 3' to the damage site (2-aPu₇) generally retain a B-like geometry (Figure 5A,C). The AP(2-aPu) substrate undergoes smaller backbone bending at the AP site and has a lower rmsd value than the AP substrate without 2-aPu (Table 4). At the same time, the individual nucleotides of the AP(2-aPu) substrate demonstrate an unusually high degree of internal flexibility that is evident from rmsf values (Table 5). Thus, we postulate that this structure can be easily deformed by the APE1 specificity loops⁶³ to rapidly form the catalytically competent complex. Supporting this prediction, the structural data prove that both the enzyme specificity and its ability to retain the reaction product until it can be passed to the next enzyme of the BER pathway are determined by specific interactions among Arg¹⁷⁷, Asn²²⁶, and Asn²²⁹ side chains and the DNA 3' region to the damage site.⁶⁴

In the case of F(2-aPu) substrate modeling, we have found the values of DNA kinking and rmsd to be comparable to those of the F substrate without 2-aPu. However, analysis of rmsf values indicates the reduced level of motion of the backbone and bases relative to AP(2-aPu) or F substrate structures. The stopped-flow assay has yielded a 5-fold decrease in the catalysis rate when switching between AP(2-aPu) and F(2-aPu) substrates and an enzyme affinity reduced by 1 order of

magnitude (Table 2). Our observations testify that these properties result from modified binding rather than from incision ability. Therefore, the relative positioning of the 2-aPu probe 3' to the F site within the duplex prevents the APE1 specificity loops from penetrating into the DNA minor and major grooves during the course substrate recognition and binding.

By summarizing our experimental and computational observations for (2-aPu)AP and (2-aPu)F substrates, we conclude that the placement of the 2-aPu₅ base slightly affects the steps of damage recognition and binding but makes the proceeding of the primary (ES) complex into the catalytically active form more difficult and substantially decreases the rate of cleavage. Indeed, DNA modeling data for these two substrates have shown an unexpectedly large kinking at the abasic site that correlates with significant distortion of the duplexes (Table 4). On the other hand, the rmsf values demonstrate an appreciable rigidity of structures, especially for the (2-aPu)AP substrate (Table 5). Therefore, this kind of DNA structure is remarkably deformed and not flexible at the same time, making it a poor substrate for APE1. According to panels B and D of Figure 5, double helices of (2-aPu)AP and (2-aPu)F substrates are bent into the major groove, giving rise to compression of the void between the abasic sugar ring and opposite C₁₉ base. In the case of the (2-aPu)F substrate, the orphan C₁₉ base was found to be stabilized in the extrahelical conformation with an rmsf of ~0.4 Å. We also observed substantial changes in the helix geometry in the bottom DNA part that is considered to be important for specific recognition by APE1.^{16,18} It, therefore, seems likely that the difficulties with formation of the catalytically competent complex arise from a complication of the APE1–major groove contacts that involve the Arg¹⁷⁷ specificity loop, Arg⁷³, Ala⁷⁴, and Lys⁷⁸ side chains interacting with the undamaged strand 3' of the AP site and Trp²⁸⁰ penetrating the abasic site void. All the structural characteristics mentioned above eventually lead to a reduction in the APE1 reaction rate as compared to those of AP(2-aPu) and F(2-aPu) substrates. It should be noted that our data are consistent with previously reported results of Dempfle and co-workers²⁶ for APE1 catalysis, which demonstrate a 4–10-fold reduction in the cleavage rate for F-containing ODNs with a 5' mismatch. In light of these findings, the 2-aPu·C base pair placed adjacent to the abasic site may be recognized by APE1 as a mismatch near the specific lesion, resulting in a substantial diminution of the reaction rate.

Using the stopped-flow fluorescence assay, we cannot accurately distinguish between the substrate incision and the nicked product release events. The decrease in the cleavage rate observed for (2-aPu)AP and (2-aPu)F substrates may be caused by a slow dissociation of the (EP) complex (Scheme 1). To test this hypothesis, we examined the affinity of APE1 for nicked DNA duplexes representing the reaction products (Figure 4 and Table 3). The results of direct fluorescence titration of the enzyme with product ODNs yielded approximately similar values of the dissociation constant (K_D^{titr}), regardless of the location of the 2-aPu probe. Thus, we suggest that a reduction in the cleavage rate observed when 2-aPu is a 5' abasic site neighbor refers to impaired incision ability rather than an enhanced APE1 affinity for this kind of DNA structure. Furthermore, the findings have evidently shown the correlation between the structural flexibility of DNA (rmsf) and the APE1 reaction rate (k_r^{SF}) (Table 5), confirming the earlier assumption that abasic DNA should be able to accommodate the bending and kinking for catalysis.⁶²

Two Independent Fluorophores Have Shown the DNA Void-Filling Process. In this work, the combination of Trp and 2-aminopurine fluorescence in the pre-steady-state stopped-flow analysis permits us to more precisely attribute each step of the kinetic mechanism to specific individual events within the enzyme–DNA complex. Figure 6 shows a graphical

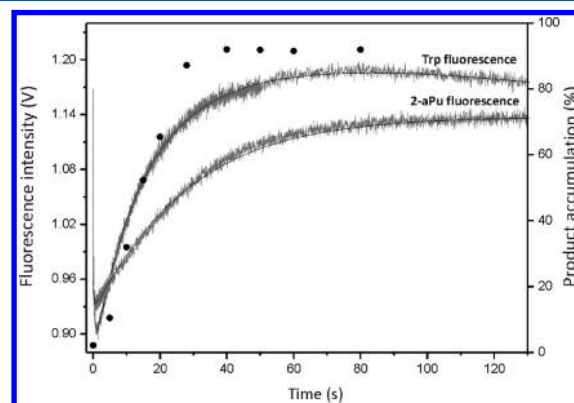


Figure 6. Comparison of stopped-flow (gray curves) and chemical quench assays (●) for interactions of equimolar amounts (1.5 μ M) of APE1 and the (2-aPu)F substrate.

comparison of the stopped-flow data followed by Trp or 2-aPu fluorescence with results of PAGE analysis for the slowest (2-aPu)F substrate. It can clearly be seen that a considerable increase in fluorescence intensity of both fluorophores coincides with the appearance of product bands in the chemical quench assay. Therefore, one can discriminate with confidence between APE1 and DNA conformational transitions before and after the cleavage step.

A careful examination of the stopped-flow data has revealed additional conformational transitions of an unknown nature within the APE1–DNA complex observed at the early stages of F(2-aPu) and (2-aPu)F substrate processing. The apparent effect on both 2-aPu and Trp fluorescence curves was marked as phase 2 (Figures 1C,D and 4C,D). The slight increase in enzyme fluorescence observed in the second step of the mechanism was similar to that of the F substrate without 2-aPu processing reported in our previous study.³⁷ In the case of (2-aPu)AP substrate processing, the discernible increase in fluorescence intensity was also found upon detection of the enzyme dynamics in the 0.04–0.2 s time interval (Figure 3B). However, the expected decrease in 2-aPu fluorescence curves was rather undetectable, complicating the quantitative analysis (Figure 1B). Figure 6 shows representative stopped-flow curves for interactions between APE1 and the (2-aPu)F substrate derived from different fluorophores. Characteristic times of appearance and disappearance of these transient states suggest that some kind of APE1 conformational change, characterized by k_2 and k_{-2} rate constants (Table 2), can induce the conformational rearrangement within the DNA substrate accompanied by a decrease in 2-aPu fluorescence. The described events within the enzyme–DNA precatalytic complex immediately result in the cleavage step and the release of incised products. To make possible assumptions about the nature of observed conformational transitions, we employed the crystallography data along with MD simulation results. It is known that the processing of the damaged DNA by DNA glycosylases or AP endonucleases is accompanied by severe DNA kinking at the site of the lesion followed by eversion of

the damaged nucleotide from the double helix into the enzyme catalytic pocket. To stabilize the precatalytic complex, we inserted specific amino acid residues further into the resulting void in the DNA helix. The stopped-flow data reported by our colleagues indicate that the DNA kinking and void-filling processes in the case of *E. coli* Fpg protein can be accordingly discerned by a sequential increase (≤ 10 ms) and decrease (~ 1 s) in the 2-aPu fluorescence signal.⁴⁴ Our data have shown a similar decrease in the 2-aPu fluorescence intensity in step 2 of the kinetic mechanism observed up to 0.2–1 s, depending on the substrate type. Given that the process of excision of a damaged base by Fpg protein is much slower than the APE1 catalytic reaction,^{65,66} we could not observe the DNA conformational change corresponding to the kinking process. For the same reason, we propose the observed induced fit of APE1 and the target DNA resulted in a more buried conformation of the abasic site region to represent insertion of the enzyme amino acids into the DNA void to stabilize the flipped-out AP site. The latter study of the role of Trp²⁸⁰ located in the vicinity of the APE1 catalytic site has revealed that this amino acid can intercalate into the abasic site void, serving as a specific “recognizer” of the lesion.²² Supporting this hypothesis, our stopped-flow data along with MD simulation results have clearly demonstrated the penetration of the enzyme’s Trp residue into the AP site void through the DNA major groove followed by stabilization of the flipped-out abasic sugar ring. The observed interactions within the precatalytic complex are the most evident for the (2-aPu)F substrate that has the lowest k_r^{SF} constant value and an extensive interval of decreases in Trp fluorescence for the steps before catalysis. On the basis of the fluorescence properties of the tryptophan side chain, we suggest that detected long quenching accompanied by specific conformational dynamics within the DNA molecule represents hydrophobic or stacking interactions between the aromatic amino acid residue and heterocyclic bases near the abasic site.

CONCLUSION

This work has expanded the scope of our previous stopped-flow study of human APE1 by applying two independent fluorescent probes for detection of DNA and protein conformational changes in real time. Employing the 2-aPu fluorescent base adjacent to the natural AP site or F along with the Trp fluorescence of the enzyme permits us to draw more precise conclusions about the nature of each stage of the previously reported kinetic mechanism. Pre-steady-state stopped-flow data have revealed a multistep character of conformational dynamics within the APE1–DNA complex. The approach applied has provided new evidence of our hypothesis that the C1'-hydroxyl moiety of the abasic sugar is important for effective catalysis. Comparison of MD simulations of DNA substrate structures with the experimental findings has proven the following tendency: the more flexible the damaged DNA duplex, the higher the rate of being processed by APE1. Taken together, the structural and pre-steady-state kinetic data evidently demonstrate the process of AP-DNA void filling through insertion of the specific amino acids into the DNA major groove during the formation of the catalytically competent enzyme–substrate complex.

ASSOCIATED CONTENT

Supporting Information

Quality of the fit estimated by inspection of the residuals (Figure S1), direct PAGE analysis of the accumulation of nicked products (Figure S2), stopped-flow traces obtained for undamaged 2-aPu-containing DNA (Figure S3), and rmsf values of abasic site nucleotides that demonstrate a lower conformational flexibility relative to that of the DNA substrates mentioned above (overall rmsf values listed in Table S1). This material is available free of charge via the Internet at <http://pubs.acs.org>.

AUTHOR INFORMATION

Corresponding Author

*Telephone: +7 383 363 51 75. Fax: +7 383 363 51 53. E-mail: fedorova@niboch.nsc.ru.

Funding

Supported in part by grants from the Siberian Branch of the Russian Academy of Sciences, the Russian Foundation for Basic Research (10-04-00070 and 12-04-00135), the Russian Ministry of Education and Science (NS-64.2012.4, State Contract 16.512.11.2073), and the Program of the Russian Government to support leading scientists (Grant 11.G34.31.0045).

Notes

The authors declare no competing financial interest.

ACKNOWLEDGMENTS

We thank S. E. Tsutakawa and Prof. J. A. Tainer for helpful comments and suggestions.

ABBREVIATIONS

APE1, AP endonuclease 1; BER, base excision repair; NIR, nucleotide incision repair; AP, apurinic/aprimidinic; F, (3-hydroxytetrahydrofuran-2-yl)methyl phosphate; 2-aPu, 2-aminopurine; ODN, oligodeoxyribonucleotide; PAGE, polyacrylamide gel electrophoresis.

REFERENCES

- (1) Demple, B., Herman, T., and Chen, D. S. (1991) Cloning and expression of APE, the cDNA encoding the major human apurinic endonuclease: Definition of a family of DNA repair enzymes. *Proc. Natl. Acad. Sci. U.S.A.* 88, 11450–11454.
- (2) Robson, C. N., and Hickson, I. D. (1991) Isolation of cDNA clones encoding a human apurinic/aprimidinic endonuclease that corrects DNA repair and mutagenesis defects in *E. coli* xth (exonuclease III) mutants. *Nucleic Acids Res.* 19, 5519–5523.
- (3) Wilson, D. M. III, and Barsky, D. (2001) The major human abasic endonuclease: Formation, consequences and repair of abasic lesions in DNA. *Mutat. Res.* 485, 283–307.
- (4) Demple, B., and Sung, J. S. (2005) Molecular and biological roles of Ape1 protein in mammalian base excision repair. *DNA Repair* 4, 1442–1449.
- (5) Nakamura, J., and Swenberg, J. A. (1999) Endogenous apurinic/aprimidinic sites in genomic DNA of mammalian tissues. *Cancer Res.* 59, 2522–2526.
- (6) Ischenko, A. A., and Saparbaev, M. K. (2002) Alternative nucleotide incision repair pathway for oxidative DNA damage. *Nature* 415, 183–187.
- (7) Abate, C., Patel, L., Rauscher, F. J. III, and Curran, T. (1990) Redox regulation of fos and jun DNA-binding activity in vitro. *Science* 249, 1157–1161.

- (8) Xanthoudakis, S., and Curran, T. (1992) Identification and characterization of Ref-1, a nuclear protein that facilitates AP-1 DNA-binding activity. *EMBO J.* 11, 653–665.
- (9) Xanthoudakis, S., Miao, G., Wang, F., Pan, Y. C., and Curran, T. (1992) Redox activation of Fos-Jun DNA binding activity is mediated by a DNA repair enzyme. *EMBO J.* 11, 3323–3335.
- (10) Xanthoudakis, S., Smeyne, R. J., Wallace, J. D., and Curran, T. (1996) The redox/DNA repair protein, Ref-1, is essential for early embryonic development in mice. *Proc. Natl. Acad. Sci. U.S.A.* 93, 8919–8923.
- (11) Gaiddon, C., Moorthy, N. C., and Prives, C. (1999) Ref-1 regulates the transactivation and pro-apoptotic functions of p53 in vivo. *EMBO J.* 18, 5609–5621.
- (12) Evans, A. R., Limp-Foster, M., and Kelley, M. R. (2000) Going APE over ref-1. *Mutat. Res.* 461, 83–108.
- (13) Kelley, M. R., and Parsons, S. H. (2001) Redox regulation of the DNA repair function of the human AP endonuclease Ape1/ref-1. *Antioxid. Redox Signaling* 3, 671–683.
- (14) Mundle, S. T., Delaney, J. C., Essigmann, J. M., and Strauss, P. R. (2009) Enzymatic mechanism of human apurinic/aprimidinic endonuclease against a THF AP site model substrate. *Biochemistry* 48, 19–26.
- (15) Gorman, M. A., Morera, S., Rothwell, D. G., de La Fortelle, E., Mol, C. D., Tainer, J. A., Hickson, I. D., and Freemont, P. S. (1997) The crystal structure of the human DNA repair endonuclease HAP1 suggests the recognition of extra-helical deoxyribose at DNA abasic sites. *EMBO J.* 16, 6548–6558.
- (16) Mol, C. D., Izumi, T., Mitra, S., and Tainer, J. A. (2000) DNA-bound structures and mutants reveal abasic DNA binding by APE1 and DNA repair coordination. *Nature* 403, 451–456.
- (17) Beernink, P. T., Segelke, B. W., Hadi, M. Z., Erzberger, J. P., Wilson, D. M. III, and Rupp, B. (2001) Two divalent metal ions in the active site of a new crystal form of human apurinic/aprimidinic endonuclease, Ape1: Implications for the catalytic mechanism. *J. Mol. Biol.* 307, 1023–1034.
- (18) Nguyen, L. H., Barsky, D., Erzberger, J. P., and Wilson, D. M. III (2000) Mapping the protein-DNA interface and the metal-binding site of the major human apurinic/aprimidinic endonuclease. *J. Mol. Biol.* 298, 447–459.
- (19) Mol, C. D., Kuo, C. F., Thayer, M. M., Cunningham, R. P., and Tainer, J. A. (1995) Structure and function of the multifunctional DNA-repair enzyme exonuclease III. *Nature* 374, 381–386.
- (20) Singer, B., and Hang, B. (1997) What structural features determine repair enzyme specificity and mechanism in chemically modified DNA? *Chem. Res. Toxicol.* 10, 713–732.
- (21) Erzberger, J. P., Barsky, D., Schärer, O. D., Colvin, M. E., and Wilson, D. M. III (1998) Elements in abasic site recognition by the major human and *Escherichia coli* apurinic/aprimidinic endonucleases. *Nucleic Acids Res.* 26, 2771–2778.
- (22) Kaneda, K., Sekiguchi, J., and Shida, T. (2006) Role of the tryptophan residue in the vicinity of the catalytic center of exonuclease III family AP endonucleases: AP site recognition mechanism. *Nucleic Acids Res.* 34, 1552–1563.
- (23) Fahrig, R., Quietzs, D., Heinrich, J. C., Heinemann, V., Boeck, S., Schmid, R. M., Praha, C., Liebert, A., Sonntag, D., Krupitza, G., and Hanel, M. (2006) RP101 improves the efficacy of chemotherapy in pancreas carcinoma cell lines and pancreatic cancer patients. *Anti-Cancer Drugs* 17, 1045–1056.
- (24) Fishel, M. L., and Kelley, M. R. (2007) The DNA base excision repair protein Ape1/Ref-1 as a therapeutic and chemopreventive target. *Mol. Aspects Med.* 28, 375–395.
- (25) Bapat, A., Glass, L. S., Luo, M., Fishel, M. L., Long, E. C., Georgiadis, M. M., and Kelley, M. R. (2010) Novel small-molecule inhibitor of apurinic/aprimidinic endonuclease 1 blocks proliferation and reduces viability of glioblastoma cells. *J. Pharmacol. Exp. Ther.* 334, 988–998.
- (26) Wilson, D. M. III, Takeshita, M., Grollman, A. P., and Demple, B. (1995) Incision activity of human apurinic endonuclease (Ape) at abasic site analogs in DNA. *J. Biol. Chem.* 270, 16002–16007.
- (27) Strauss, P. R., Beard, W. A., Patterson, T. A., and Wilson, S. H. (1997) Substrate binding by human apurinic/aprimidinic endonuclease indicates a Briggs-Haldane mechanism. *J. Biol. Chem.* 272, 1302–1307.
- (28) Mundle, S. T., Fattal, M. H., Melo, L. F., Coriolan, J. D., O'Regan, N. E., and Strauss, P. R. (2004) Novel role of tyrosine in catalysis by human AP endonuclease 1. *DNA Repair* 3, 1447–1455.
- (29) Marenstein, D. R., Wilson, D. M. III, and Teebor, G. W. (2004) Human AP endonuclease (Ape1) demonstrates endonucleolytic activity against AP sites in single-stranded DNA. *DNA Repair* 3, 527–533.
- (30) Masuda, Y., Bennett, R. A., and Demple, B. (1998) Dynamics of the interaction of human apurinic endonuclease (Ape1) with its substrate and product. *J. Biol. Chem.* 273, 30352–30359.
- (31) Maher, R. L., and Bloom, L. B. (2007) Pre-steady-state kinetic characterization of the AP endonuclease activity of human AP endonuclease 1. *J. Biol. Chem.* 282, 30577–30585.
- (32) Johnson, K. A. (1998) Advances in transient-state kinetics. *Curr. Opin. Biotechnol.* 9, 87–89.
- (33) Fedorova, O. S., Nevinsky, G. A., Koval, V. V., Ishchenko, A. A., Vasilenko, N. L., and Douglas, K. T. (2002) Stopped-flow kinetic studies of the interaction between *Escherichia coli* Fpg protein and DNA substrates. *Biochemistry* 41, 1520–1528.
- (34) Koval, V. V., Kuznetsov, N. A., Zharkov, D. O., Ishchenko, A. A., Douglas, K. T., Nevinsky, G. A., and Fedorova, O. S. (2004) Pre-steady-state kinetics shows differences in processing of various DNA lesions by *Escherichia coli* formamidopyrimidine-DNA glycosylase. *Nucleic Acids Res.* 32, 926–935.
- (35) Zhai, J., and Hingorani, M. M. (2010) *Saccharomyces cerevisiae* Msh2-Msh6 DNA binding kinetics reveal a mechanism of targeting sites for DNA mismatch repair. *Proc. Natl. Acad. Sci. U.S.A.* 107, 680–685.
- (36) Trakselis, M. A., Alley, S. C., Abel-Santos, E., and Benkovic, S. J. (2001) Creating a dynamic picture of the sliding clamp during T4 DNA polymerase holoenzyme assembly by using fluorescence resonance energy transfer. *Proc. Natl. Acad. Sci. U.S.A.* 98, 8368–8375.
- (37) Kanazhevskaya, L. Y., Koval, V. V., Zharkov, D. O., Strauss, P. R., and Fedorova, O. S. (2010) Conformational transitions in human AP endonuclease 1 and its active site mutant during abasic site repair. *Biochemistry* 49, 6451–6461.
- (38) Hoehn, S. T., Turner, C. J., and Stubbe, J. (2001) Solution structure of an oligonucleotide containing an abasic site: Evidence for an unusual deoxyribose conformation. *Nucleic Acids Res.* 29, 3413–3423.
- (39) Breslauer, K. J., Frank, R., Blocker, H., and Marky, L. A. (1986) Predicting DNA duplex stability from the base sequence. *Proc. Natl. Acad. Sci. U.S.A.* 83, 3746–3750.
- (40) Gelfand, C. A., Plum, G. E., Grollman, A. P., Johnson, F., and Breslauer, K. J. (1998) Thermodynamic consequences of an abasic lesion in duplex DNA are strongly dependent on base sequence. *Biochemistry* 37, 7321–7327.
- (41) Sugimoto, N., Nakano, S., Yoneyama, M., and Honda, K. (1996) Improved thermodynamic parameters and helix initiation factor to predict stability of DNA duplexes. *Nucleic Acids Res.* 24, 4501–4505.
- (42) Dunlap, C. A., and Tsai, M.-D. (2002) Use of 2-Aminopurine and Tryptophan Fluorescence as Probes in Kinetic Analyses of DNA Polymerase β . *Biochemistry* 41, 11226–11235.
- (43) Kuzmick, P. (1996) Program DYNAPIT for the analysis of enzyme kinetic data: Application to HIV proteinase. *Anal. Biochem.* 237, 260–273.
- (44) Kuznetsov, N. A., Koval, V. V., Zharkov, D. O., Vorobjev, Y. N., Nevinsky, G. A., Douglas, K. T., and Fedorova, O. S. (2007) Pre-steady-state kinetic study of substrate specificity of *Escherichia coli* formamidopyrimidine-DNA glycosylase. *Biochemistry* 46, 424–435.
- (45) Popov, A. V., and Vorob'ev, Iu. N. (2010) GUI-BioPASED program for molecular dynamics modelling of biopolymers with a graphical user interface. *Mol. Biol. (Moscow)* 44, 735–742.
- (46) Cornell, W. D., Cieplak, P., Bayly, C. I., Gould, I. R., Merz, K. M., Ferguson, D. M., Spellmeyer, D. C., Fox, T., Caldwell, J. W., and

Kollman, P. A. (1995) A second generation force field for the simulation of proteins, nucleic acids, and organic molecules. *J. Am. Chem. Soc.* 117, 5179–5197.

(47) Lazaridis, T., and Karplus, M. (1999) Effective energy function for proteins in solution. *Proteins* 35, 133–152.

(48) Humphrey, W., Dalke, A., and Schulten, K. (1996) VMD: Visual molecular dynamics. *J. Mol. Graphics* 14, 27–38.

(49) Barsky, D., Foloppe, N., Ahmadi, S., Wilson, D. M., and MacKerell, A. D. (2000) New insights into the structure of abasic DNA from molecular dynamics simulations. *Nucleic Acids Res.* 28, 2613–2626.

(50) Law, S. M., Eritja, R., Goodman, M. F., and Breslauer, K. J. (1996) Spectroscopic and calorimetric characterizations of DNA duplexes containing 2-aminopurine. *Biochemistry* 35, 12329–12337.

(51) Jean, J. M., and Hall, K. B. (2002) 2-Aminopurine electronic structure and fluorescence properties in DNA. *Biochemistry* 41, 13152–13161.

(52) Stivers, J. T. (1998) 2-Aminopurine fluorescence studies of base stacking interactions at abasic sites in DNA: Metal-ion and base sequence effects. *Nucleic Acids Res.* 26, 3837–3844.

(53) Rachofsky, E. L., Seibert, E., Stivers, J. T., Osman, R., and Ross, J. B. (2001) Conformation and dynamics of abasic sites in DNA investigated by time-resolved fluorescence of 2-aminopurine. *Biochemistry* 40, 957–967.

(54) Sowers, L. C., Fazakerley, G. V., Eritja, R., Kaplan, B. E., and Goodman, M. F. (1986) Base pairing and mutagenesis: Observation of a protonated base pair between 2-aminopurine and cytosine in an oligonucleotide by proton NMR. *Proc. Natl. Acad. Sci. U.S.A.* 83, 5434–5438.

(55) Timofeyeva, N. A., Koval, V. V., Knorre, D. G., Zharkov, D. O., Saparbaev, M. K., Ishchenko, A. A., and Fedorova, O. S. (2009) Conformational dynamics of human AP endonuclease in base excision and nucleotide incision repair pathways. *J. Biomol. Struct. Dyn.* 26, 637–652.

(56) Takeshita, M., Chang, C. N., Johnson, F., Will, S., and Grollman, A. P. (1987) Oligodeoxynucleotides containing synthetic abasic sites. Model substrates for DNA polymerases and apurinic/apyrimidinic endonucleases. *J. Biol. Chem.* 262, 10171–10179.

(57) Berquist, B. R., McNeill, D. R., and Wilson, D. M. III (2008) Characterization of abasic endonuclease activity of human Ape1 on alternative substrates, as well as effects of ATP and sequence context on AP site incision. *J. Mol. Biol.* 379, 17–27.

(58) Kuznetsov, N. A., Koval, V. V., Nevinsky, G. A., Douglas, K. T., Zharkov, D. O., and Fedorova, O. S. (2007) Kinetic conformational analysis of human 8-oxoguanine-DNA glycosylase. *J. Biol. Chem.* 282, 1029–1038.

(59) Coppel, Y., Berthet, N., Coulombeau, C., Garcia, J., and Lhomme, J. (1997) Solution conformation of an abasic DNA undecamer duplex d(CGCACXCACGC) × d(GCGTGTGTGCG): The unpaired thymine stacks inside the helix. *Biochemistry* 36, 4817–4830.

(60) Fagan, P. A., Fabrega, C., Eritja, R., Goodman, M. F., and Wemmer, D. E. (1996) NMR study of the conformation of the 2-aminopurine:cytosine mismatch in DNA. *Biochemistry* 35, 4026–4033.

(61) Wilde, J. A., Bolton, P. H., Mazumder, A., Manoharan, M., and Gerlt, J. A. (1989) Characterization of the Equilibrating Forms of the Aldehydic Abasic Site in Duplex DNA by O-17 NMR. *J. Am. Chem. Soc.* 111, 1894–1896.

(62) Oezguen, N., Schein, C. H., Peddi, S. R., Power, T. D., Izumi, T., and Braun, W. (2007) A “moving metal mechanism” for substrate cleavage by the DNA repair endonuclease APE-1. *Proteins* 68, 313–323.

(63) Mol, C. D., Hosfield, D. J., and Tainer, J. A. (2000) Abasic site recognition by two apurinic/apyrimidinic endonuclease families in DNA base excision repair: The 3′ ends justify the means. *Mutat. Res.* 460, 211–229.

(64) Izumi, T., Schein, C. H., Oezguen, N., Feng, Y., and Braun, W. (2004) Effects of backbone contacts 3′ to the abasic site on the

cleavage and the product binding by human apurinic/apyrimidinic endonuclease (APE1). *Biochemistry* 43, 684–689.

(65) Audebert, M., Radicella, J. P., and Dizdaroglu, M. (2000) Effect of single mutations in the OGG1 gene found in human tumors on the substrate specificity of the Ogg1 protein. *Nucleic Acids Res.* 28, 2672–2678.

(66) Starostin, K. V., Ishchenko, A. A., Zharkov, D. O., Buneva, V. N., and Nevinskii, G. A. (2007) Interactions of pro- and eukaryotic DNA repair enzymes with oligodeoxyribonucleotides containing clustered lesions. *Mol. Biol. (Moscow)* 41, 112–120.